

Stochastic Mean-Field Theory: Method and Application to the Disordered Bose-Hubbard Model at Finite Temperature and Speckle Disorder

Ulf Bissbort,¹ Ronny Thomale,² and Walter Hofstetter¹

¹*Institut für Theoretische Physik, Johann Wolfgang Goethe-Universität, 60438 Frankfurt/Main, Germany*

²*Department of Physics, Princeton University, Princeton, NJ 08544*

(Dated: June 15, 2018)

We discuss the stochastic mean-field theory (SMFT) method which is a new approach for describing disordered Bose systems in the thermodynamic limit including localization and dimensional effects. We explicate the method in detail and apply it to the disordered Bose-Hubbard model at finite temperature, with on-site box disorder, as well as experimentally relevant unbounded speckle disorder. We find that disorder-induced condensation and reentrant behavior at constant filling are only possible at low temperatures, beyond the reach of current experiments¹⁷. Including off-diagonal hopping disorder as well, we investigate its effect on the phase diagram in addition to pure on-site disorder. To make contact to present experiments on a quantitative level, we also combine SMFT with an LDA approach and obtain the condensate fraction in the presence of an external trapping potential.

PACS numbers: 67.85.Hj, 03.75.Hh, 71.55.Jv

I. INTRODUCTION

The interplay between disorder and interactions in Bose systems has been a vital field of research in condensed matter both in theory and experiment. The line of investigation was mainly initiated by the seminal work of Fisher et al.¹, who first provided a detailed study of localization of interacting bosons in a random potential, which led to the notion of the superfluid-insulator transition and the Bose glass (BG). While disorder effects in Fermi systems are relevant to a broad range of experimentally accessible scenarios like correlated electron systems, the status was less diverse for Bose systems for a considerable time period, as superfluid ⁴He situated in random pores of Vycor had been the predominant setup which could be studied with sufficient precision². This changed dramatically when the realization of the superfluid-Mott insulator transition of ultracold bosonic atoms in an optical lattice opened up a new field of investigation^{3,5}. In particular, optical lattices provide a relatively pure and tunable simulation of effective models used to describe solid state systems⁶, where effects like disorder can also be realized in a controlled manner. While several alternative realizations of disorder in optical lattices, such as multichromatic lattices with non-commensurate wavelengths⁷⁻¹⁰ or multi-species gases with strongly differing tunneling rates^{11,12} have been proposed recently, speckle laser patterns are probably by now one of the most efficient methods to establish disorder in cold atoms^{13-17,30}. Therein, it is possible to combine the speckle beam with the remaining apparatus of the optical lattice to simulate disordered lattice systems with a high tuning accuracy and without other side effects.

A variety of theoretical approaches⁴ has by now been applied to the disordered Bose Hubbard model (BHM), first introduced for ultracold atoms by Jaksch et al.⁵,

which is described by the Hamiltonian

$$\mathcal{H}_{\text{BH}} = -J \sum_{\langle i,j \rangle} (b_i^\dagger b_j + \text{h.c.}) + \sum_i (\epsilon_i - \mu) n_i + \frac{U}{2} \sum_i n_i (n_i - 1), \quad (1)$$

where b_i (b_i^\dagger) annihilates (creates) a particle in the lowest band Wannier state at site i , $n_i = b_i^\dagger b_i$ is the local particle number operator, J denotes the nearest neighbor hopping energy in the lowest band, and μ is the chemical potential. ϵ_i is an on-site energy shift, which in our case is a spatially uncorrelated random variable drawn from a distribution $p(\epsilon)$ and U is the on-site repulsive interaction. The subscript $\langle i, j \rangle$ indicates the sum over all neighboring pairs of sites. Unless stated otherwise, we use the unit $U = 1$.

Several quantum phases can exist within this model, such as the Mott insulator (MI), the Bose glass, the condensed phase, commonly referred to as the superfluid (SF), as well as the normal phase at finite temperature. The transitions between these phases, which constitute some of the first experimentally feasible quantum phase transitions in bosonic systems, have attracted much attention. Numerically, a powerful approach is Quantum Monte Carlo¹⁸⁻²⁵ (QMC). While MI and SF phase can be characterized efficiently¹⁸, the BG phase and the vicinities of the transition lines are significantly more complicated to be adequately described. The main reason is that for finite size calculations in general, it is problematic to capture the correct description of the phase borders, which are essentially dominated by rare events, which is also a problem for QMC methods. In most cases, exact diagonalization studies are simply inadequate due to limited size and number of particles, which often obscures essential physics (however, there may appear aspects that can indeed be suitably captured by small clusters²⁶). On the other hand, with a similar range of

treatable system sizes as QMC, density matrix renormalization group (DMRG) is an efficient complementary method²⁷. However, DMRG is currently only applicable in one spatial dimension and thus does not allow for a description of effects in higher dimensional lattices. Analytically, renormalization group analysis^{28–30}, slave boson theory³¹, the strong coupling approach³², and various different kinds of mean field theory descendants have been applied to the BHM with and without disorder^{33–40}. Arithmetically averaged mean-field theories, on the other hand, are incapable of resolving the BG phase at all for $T = 0$ ³⁷, but also for $T > 0$ impose an unphysically strong phase coherence, leading to an overestimation of the SF phase. Other methods like the random phase approximation (RPA) which has successfully been applied to the system without disorder^{35,36} again suffer from finite size effects for the BHM with disorder, as the absence of translational symmetry constrains its applicability to much smaller system sizes.

To circumvent this type of problems in describing the different phases of the disordered BHM, we use the SMFT which has been previously introduced and applied to the disordered BHM at zero temperature³⁸. There, it was found that the method efficiently describes localization, is both valid in high dimensions and in the thermodynamic limit, capturing rare events with their respective statistical weight and includes dimensional effects. In particular, it was found that at fixed μ , there exists a critical hopping strength, above which the system remains superfluid for arbitrarily strong disorder.

In this article, we present the SMFT in detail and investigate how the results found for the disordered BHM at zero temperature are modified at finite temperature. In addition to prototypical box disorder, we consider exponential speckle disorder to better simulate systems realized in current experiments. Here, the results are qualitatively different in the sense that for any finite disorder strength the MI gives way to the BG.

The paper is organized as follows: In Sec. II, the SMFT is explained in detail. First the general scope is outlined, followed by the definition of quantities computed within SMFT, such as compressibility, local Greens functions and condensate fraction. In Sec. III, the essential results for the disordered BHM at $T = 0$ are given, followed by the extension of the SMFT calculations to $T \neq 0$. In Sec. IV we extend the results presented for box disorder³⁸, including finite temperature effects. Alternative types of disorder, in particular disorder induced by speckle lasers are discussed for the BHM in Sec. V. As another possible source of disorder, we discuss the effect of kinetic (hopping) disorder in the BHM in Sec. VB. However, we find no sensible dependence of the system on this parameter. The applicability of these results to current experiments essentially relies on the estimate of experimental temperature, which is discussed on in Sec. VIA. We find that the experimentally realized temperatures are still far above the regime for which we resolve the previously stated interesting phenomena, such as disorder-

induced condensation and reentrant behavior. LDA + SMFT calculations are discussed in Sec. VIB to provide a closer connection to experimentally measurable quantities. In Sec. VII, we conclude that the SMFT is an efficient theoretical approach to disordered Bose systems and promises an adequate description of ongoing experiments.

II. METHOD

As pointed out previously^{1,37}, performing a self-consistent disorder average over all local on-site energies is not sufficient to generally describe the insulating Bose-glass phase. From spatially resolved bosonic Gutzwiller calculations, it becomes apparent that this method overestimates long range correlations, predicting the formation of a global condensate into a single particle orbital which consists of the superposition of a large (extensive) number of distinct localized single particle states. In the true Bose glass phase, off-diagonal long range order does not prevail and a large (although not extensive) number of particles may occupy each of these localized modes independently, leading to a condensate fraction $f_c = 0$ in the thermodynamic limit. However, by imposing phase rigidity and averaging over all mean-field parameters $\psi_i = \langle b_i \rangle$ with the same complex phase, the spatially resolved (as well as the arithmetically averaged) Gutzwiller theory leads to a finite average mean-field parameter (MFP) and a finite condensate fraction $f_c = \overline{\langle b \rangle}^2 / \overline{\langle b^\dagger b \rangle}$ in the expected BG regime.

In contrast to the approaches mentioned above, the SMFT is constructed as a single-site theory in the thermodynamic limit, which effectively describes fluctuations in the MFPs using a probability density function (PDF) $P(\psi)$. Set up in this fashion, the SMFT method is not restricted to incorporating disorder fluctuations only, but may also be a powerful approach to treat fluctuations of different origins, such as of thermal or quantum type in a unified framework. The concept of approximating quantum mechanical operators by random variables has been applied previously in a variety of physical scenarios^{41–43}. In this paper, we will focus on disorder-induced fluctuations at finite temperature. In this section, we will discuss the construction of SMFT in detail, concentrating on the case of including on-site disorder. Extensions of including disorder in the hopping parameter J or thermal fluctuations explicitly are discussed in Sec. VB and App. F respectively.

The central quantity, which effectively describes a disordered bosonic lattice gas in the thermodynamic limit is the probability distribution $P(\psi)$. It is assumed to be equal for all sites and in particular independent of the nearest neighbors' on-site energies. The validity of this assumption has been checked using spatially resolved mean-field theory, which is known to become exact in the non-interacting limit, while retaining interaction effects beyond Gross-Pitaevskii theory for finite U/J . It

is found that it yields correlation coefficients below 0.05 in all regimes considered³⁸, justifying the above assumption. The aim of SMFT is to find a self-consistent solution for $P(\psi)$, which is restricted and uniquely specified by self-consistency equations and minimization of energy.

Consider a cluster of lattice sites composed of a central site i and Z (the coordination number) nearest neighbors, where the corresponding part of the Hamiltonian (1) contains the operators on site i within the bosonic Gutzwiller approximation^{1,33–35}:

$$\begin{aligned} \mathcal{H}_i^{(\text{MF})} = & -J \sum_{\text{n.n. } j} (\psi_j^* b_i + \psi_j b_i^\dagger - \psi_j^* \psi_i) \\ & + (\epsilon_i - \mu) b_i^\dagger b_i + \frac{U}{2} b_i^\dagger b_i^\dagger b_i b_i. \end{aligned} \quad (2)$$

Within this approximation, the site i is coupled to (and the sum extends over) the nearest neighbors via the scalar MFPs $\psi_j = \langle b_j \rangle$, which are random variables within SMFT. Due to global particle number conservation, the MFPs can all be chosen to be real and positive, as any variation in complex phase corresponds to a boost in local kinetic energy. The expectation value $\langle b_j \rangle$ is to be evaluated in the local ground state for $T = 0$ or taking the thermal trace for $T > 0$. Thermal fluctuations can, however, also be incorporated on an explicit stochastic level in the distribution $P(\psi)$ within SMFT, as discussed in App. F. Inspecting the Hamiltonian (2), it does not depend on the ψ_j 's individually, but only on the scaled sum

$$\eta_i = J \sum_{\text{n.n. } j} \psi_j. \quad (3)$$

Since the ψ_j 's (and in the hopping disorder Sec. VB also J) are random variables, the newly defined quantity η_i is also a random variable obeying some distribution $Q(\eta)$. As discussed above, the random variables ψ_j are assumed independent within SMFT, allowing us to express the distribution $Q(\eta)$ by a Z -fold scaled convolution

$$\begin{aligned} Q(\eta) = & \int_0^\infty d\psi_1 P(\psi_1) \dots \int_0^\infty d\psi_Z P(\psi_Z) \\ & \times \delta\left(\eta - J \sum_{m=1}^Z \psi_m\right). \end{aligned} \quad (4)$$

Making use of the convolution theorem, this can be reduced to two one-dimensional Fourier transforms by introducing the characteristic function

$$\varphi(t) = \int d\psi P(\psi) e^{it\psi}, \quad (5)$$

in terms of which the function Q can be expressed as

$$Q(\eta) = \frac{1}{2\pi J} \int dt [\varphi(t)]^Z e^{-it\eta/J}. \quad (6)$$

This can be calculated efficiently for arbitrary coordination numbers Z using the FFT algorithm. The numerical procedure is discussed in App. A.

The self-consistency condition can now be formulated in the following way: If the on-site energy ϵ is randomly drawn from $p(\epsilon)$ and ψ_j is randomly drawn from the self-consistently determined distribution $P(\psi)$ for each of the Z nearest neighbors, this defines the single site Hamiltonian (2), which can be diagonalized providing the ground state $|\text{g.s.}(\epsilon, \eta)\rangle$. From there, a new MFP $\langle \text{g.s.}(\epsilon, \eta) | b | \text{g.s.}(\epsilon, \eta) \rangle$ can be calculated, with the self-consistency requiring the distribution of this new random variable to be exactly the distribution $P(\psi)$ we initially assumed for the neighboring ψ_j 's.

To cast this condition into functional form for a probability distribution in the thermodynamic limit (i.e. for an infinitely large system at fixed density), we first define the function

$$g(\mu - \epsilon, \eta) = \langle \text{g.s.}(\mu - \epsilon, \eta) | b | \text{g.s.}(\mu - \epsilon, \eta) \rangle, \quad (7)$$

where $|\text{g.s.}(\mu - \epsilon, \eta)\rangle$ is the ground state of $\mathcal{H}_i^{(\text{MF})}(\mu - \epsilon, \eta)$ given in (2).

It is useful to introduce the *conditional* PDF, which is a function of η and ψ , giving the probability density for a specified value ψ if the value of η is fixed and ϵ is distributed according to $p(\epsilon)$. This can be obtained by using the transformation property of a PDF under a variable transform and takes the form

$$\begin{aligned} \tilde{P}(\psi|\eta) = & \sum_{i | g(\mu - \epsilon_i, \eta) = \psi} \left| \left(\frac{\partial g(\mu', \eta)}{\partial \mu'} \right)_{\mu' = \mu - \epsilon_i} \right|^{-1} p(\epsilon_i) \\ = & \frac{d}{d\psi} \int d\epsilon p(\epsilon) \Theta(\psi - g(\mu - \epsilon, \eta)). \end{aligned} \quad (8)$$

This function does not obey any self-consistency condition and can be evaluated directly, which is the first step in finding $P(\psi)$. Remembering that the relation between $Q(\eta)$ and $P(\psi)$ is given by (4), so that we can express the self-consistency condition as

$$P(\psi) = \int d\eta Q(\eta) \tilde{P}(\psi|\eta). \quad (9)$$

The right hand side can be understood as follows: for every fixed η we have a PDF $P(\psi|\eta)$, which yields a contribution with the respective weight $Q(\eta)$, leading to a marginal distribution for the considered site. If this agrees with the initially assumed distribution $P(\psi)$, a self consistent solution has been found.

Once this is determined, expectation values of local, self-averaging operators \hat{A} can be directly be determined by

$$\langle \hat{A} \rangle = \text{Tr}(\varrho(\beta)), \quad (10)$$

where

$$\varrho(\beta) = \int d\epsilon p(\epsilon) \int d\eta Q(\eta) \frac{e^{-\beta \mathcal{H}_i^{(\text{MF})}(\mu - \epsilon, \eta)}}{\text{Tr}\left(e^{-\beta \mathcal{H}_i^{(\text{MF})}(\mu - \epsilon, \eta)}\right)} \quad (11)$$

is an effective disorder averaged density operator, incorporating thermal, on-site energy and MFP fluctuations, depending explicitly on $p(\epsilon)$ and the self-consistently determined $Q(\eta)$.

A. Numerical solution

To solve the SMFT equations numerically, we iterate the self-consistency equations on a discretized grid for ψ , consisting of a superposition of a variable number of equidistantly spaced grids, as explained in App. A. For every fixed set of physical parameters, we first numerically determine the conditional cumulative density distribution function $F(\psi|\eta) = \int_0^\psi d\psi' P(\psi'|\eta)$ for all values of η and ψ which constitute the numerical grids for $Q(\eta)$ and $P(\psi)$ respectively (discussed in App. B). Working with the cumulative distribution on a numerical level, as opposed to the PDF itself, is far more controlled and circumvents divergences in the PDF $P(\psi)$, but also in the conditional PDF $P(\psi|\eta)$. The self-consistency condition (9) is not influenced by this approach. As can be seen by inspection, the insulating solution $P(\epsilon) = \delta(\epsilon)$ is always a self-consistent solution, equivalent to the $\psi = 0$ solution in the single site theory. However, in the SF regime, there also exists a second, non-trivial self-consistent solution, which corresponds to a lower grand canonical potential and is therefore the physical solution in this case. Furthermore, the physical solution is always found to be the attractive fixed point of the self-consistency mapping in the space of probability distributions, i.e. if the iteration procedure is started at any $P(\psi) \neq \delta(\psi)$, the successive distributions continuously converge towards the physical distribution.

We start the iterative procedure with an initial PDF $P^{(0)}(\psi)$, where all the weight is distributed at small, but non-zero values of ψ , assuring fast convergence in the insulating state and in the vicinity of the phase border. The distribution in the i -th iteration step for the scaled sum of MFPs from the nearest neighboring sites $Q^{(i)}(\eta)$ is calculated from $P^{(i)}(\psi)$ using the convolution theorem for independent random variables and the FFT algorithm (see App. A). The new distribution $P^{(i+1)}(\psi)$ is then obtained by integration over η . Numerically this is done by using the trapezoidal rule, as we found that using higher order techniques, such as Simpson's rule, is not robust and lead to incorrect results if δ -peaks appear in the PDF.

In the vicinity of the phase border, the computational effort increases due to two effects. Firstly, the convergence is critically slowed down, increasing the required number of iterations. Secondly, the discretization of the ψ -grid plays an ever increasing role and in some parameter regimes directly on the outside of the MI lobes, where the converged distributions are very close to a δ -peak at $\psi = 0$, the numerically determined form of the distributions depends on the discretization (resolution), which is clearly unphysical. In these cases, we have to

determine $P(\psi)$ by examining a sequence of converged distributions at ever increasing resolution and define the physical distribution as the limit of this sequence.

III. PHASES OF THE DISORDERED BHM

A. Phases at $T = 0$

For the disordered BHM, three different phases exist at zero temperature: A Mott insulating state, where number fluctuations are suppressed and the particles are localized due to a repulsive interaction. This state exhibits a finite energy gap of order U , thus the single-particle density of states (DOS) at $\omega = 0$ vanishes and the state is incompressible.

If tunneling-induced delocalization dominates, the system is in a condensate (SF) phase, where a macroscopic number of particles can lower their energy by condensing into one single-particle state, thus exhibiting quantum coherence and leading to a finite condensate fraction. Within a grand-canonical mean-field description, this phase breaks the $U(1)$ -symmetry of the BH Hamiltonian (1) and leads to a non-zero order parameter. The phase border from the SF to any of the insulating phases is thus determined by SMFT, where finite weight in $P(\psi)$ moves to finite values of ψ .

Finally, there is the Bose glass phase, where particles are localized by an interplay of disorder and interactions. However, there exists no single particle state which is occupied macroscopically and thus the BG is not a condensate, i.e. the condensate fraction vanishes ($f_c = 0$). However, there does exist an extensive number of localized single particle states, each of which is occupied by an arbitrarily large, but not macroscopic number of particles. This may be understood as a highly fragmented system of *incoherent* localized 'non-macroscopic quasi-condensates'.

The transition from a BG to a MI is not determined from the self-consistent distribution $P(\psi)$, but by analyzing the compressibility κ or the single particle DOS.

We consider the latter quantity within two frameworks:

1. Considering the purely sing site particle- and hole excitations as specified in³⁷. The BG extends over the region where $P(\psi) = \delta(\psi)$ and values of the chemical potential $\mu \in \{m + \epsilon | m \in \mathbb{N}, \epsilon \in \mathbb{R}, p(\epsilon) > 0\}$, i.e. the borders are independent of J and a direct MI-SF transition is possible.
2. A more detailed analysis presented in^{24,32} relies on the analysis of an effective Hamiltonian in the subspaces of localized single particle- and hole excitations. For finite hopping J in the pure system, these hybridize, lifting the degeneracy and form superpositions with quantum numbers k . Increasing (decreasing) μ/U , the Mott insulating state remains the ground state until the energy difference between

the MI state and the $k = 0$ particle (hole) state vanishes, at which point particles delocalize and condense into these states. Now let us return to the disordered case: here the local particle (hole) excitations will not hybridize into fully delocalized states with well-defined quasi-momentum k , but into inhomogeneous states, which depend on the individual disorder configuration. It is however possible to make exact statements about the eigen-energy spectrum for a disordered system in the thermodynamic limit: The lowest kinetic energy is obtained in locally homogeneous regions and approaches the energy of the $k = 0$ particle (hole) state of the pure system, as the size of this locally homogeneous Lifshitz region increases. Furthermore, scaling predicts that the dependence of the kinetic energy on the specific boundaries to the Lifshitz region will reduce, as the size of the region increases. On the other hand, the potential energy of the particle (hole) state is minimized, when the local on-site energy takes on the lowest (highest) possible value over the whole region, i.e. lies at the extrema of $p(\epsilon)$. Therefore, upper (lower) phase boundary of the Mott lobe in the disordered system is obtained by shifting the upper (lower) boundary down (up) by $\max(\{\epsilon|p(\epsilon) > 0\})$ ($\min(\{\epsilon|p(\epsilon) > 0\})$). The MI for box disorder in 3 dimension at $T = 0$ obtained by strong coupling theory using this criterion, is the area enclosed by the orange phase boundaries in Fig. 3. The insulating region outside of these lobes, bounded from the SF by the dashed white lines, corresponds to the BG. Using this criterion, the transition from MI to SF always occurs through the BG phase for box disorder within SMFT.

B. Phases at $T > 0$

At finite temperature $T > 0$, the system is always compressible and the incompressible Mott insulator is replaced by a normal (non-superfluid) phase with a thermally induced compressibility. A central statement in³⁷ is, that the disorder-averaged single particle DOS calculated by considering purely local excitations only, allows for a clear distinction at $T > 0$ between the BG and the normal phase, as it is zero in the latter. However, when considering delocalized excitations in the particle and hole sector, this statement holds no longer, as there are generally degenerate states in the N -particle particle-hole band and the particle (hole) band in the $N+1$ sector (or the $N-1$ sector for the hole band), which can be seen from the single particle DOS in the Lehmann represen-

tation

$$\rho(\omega) = \frac{1}{Z_c} \sum_{l,l',k} e^{-\beta E_l^{(N)}} \left[|\varphi_{l'}^{(l,k)}|^2 \delta(\omega - (E_{l'}^{(N+1)} - E_l^{(N)})) + |\gamma_{l'}^{(l,k)}|^2 \delta(\omega - (E_l^{(N)} - E_{l'}^{(N-1)})) \right]. \quad (12)$$

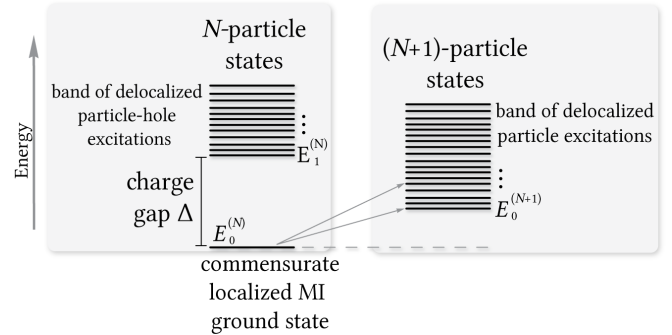


FIG. 1: Energy structure of the BHM for large U/J without disorder. The levels correspond to the energies of the exact many-particle energy eigenstates of the system with interactions. Due to the $U(1)$ -symmetry the energy eigenstates can be chosen to be of well-defined particle number. For commensurate particle number N , the ground state (MI) is separated from a band of particle-hole excitations by a charge gap, while for $N + 1$ particles, all eigenstates are delocalized, forming a band of hybridized particle states. At $T = 0$, the single particle DOS has finite weight at frequencies corresponding to energy differences $E_i^{(N+1)} - E_0^{(N)}$ of transitions between N and $N + 1$ states. At $T > 0$ transitions between different excited states also contribute, causing the gap to vanish if the two bands overlap and the respective matrix elements do not vanish.

Here, $E_l^{(N)}$ denotes the energy of the l^{th} many-particle eigenstate $|\psi_l^{(N)}\rangle$ of H_{BH} , which can always be chosen to have well-defined particle number N , since $[\mathcal{H}_{BH}, \hat{N}] = 0$, while l is a label for the eigenstate in this subspace. $\varphi_{l'}^{(l,k)} = \langle \psi_{l'}^{(N+1)} | b_k^\dagger | \psi_l^{(N)} \rangle$ and $\gamma_{l'}^{(l,k)} = \langle \psi_{l'}^{(N+1)} | b_k | \psi_l^{(N)} \rangle$ are the amplitudes for the various possible transitions. If the system is in a Mott insulating state (considering no disorder for the clarification of this argument) as shown in Fig. III B, the ground state with N particles is separated from a band of particle-hole excited states by a gap $\delta(J, U)$ (corresponding to the height of the Mott lobe at the respective J/U). As transitions between various excited states can also occur at finite temperature, the SPDOS thus vanishes if the particle-hole band with N particles, overlaps with the particle- or hole band containing $N + 1$ or $N - 1$ particles, but the weight is suppressed exponentially by δ/T . We thus conjecture, that the BG and the normal phase are not fundamentally distinguishable, and only connected by a crossover.

Following along the lines of³⁷, we use the disorder averaged local single particle density of states (DOS) at zero frequency $\bar{\rho}(\omega = 0)$ (see Eq. (E4), (E5)), to determine the normal phase / BG crossover at finite T . In the presence of disorder the SPDOS containing localized excitations can be calculated explicitly from the local Green's function in this regime (see App. E) and leads to

$$\begin{aligned} \bar{\rho}(\omega, \mu, \Delta, \beta) &= \int d\epsilon p(\epsilon) \frac{1}{Z(\mu - \epsilon)} \\ &\times \sum_{m=0}^{\infty} e^{-\beta(\frac{U}{2}m(m-1) - \mu m + \epsilon m)} [(m+1)\delta(\omega - Um + \mu - \epsilon) \\ &+ m\delta(\omega - U(m-1) + \mu - \epsilon)]. \end{aligned} \quad (13)$$

$Z(\mu')$ is the local partition function at an effective chemical potential μ' and the two δ -distributions correspond to local particle and hole excitations respectively. Using this criterion leads to an overestimation of the MI / normal phase over the BG and thereby an absence of the BG phase around the tips of the Mott lobes.

C. Deviations in Finite Size Systems

Although phase transitions are, strictly speaking, only well defined in the thermodynamic limit, crossovers observed in current experiments may indicate phase borders that do not coincide with the borders obtained in systems of infinite size. As discussed above and in^{24,32}, the MI/BG phase borders in an infinitely large disordered system simply correspond to the shifted phase borders of the pure system. This argument relies on the existence of arbitrarily large Lifshitz regions, which is clearly no longer given for finite systems. The phase diagram for a finite system therefore strongly depends on the specific disorder realization, with the critical values for the phase borders becoming random variables. Therefore, a better question to ask for a finite system for instance is: For a randomly chosen disorder realization in a system consisting of L sites, what is the probability P_g that the energy gap will be lower than a given value D ? In the limit of $J/U \rightarrow 0$ this probability is given by

$$P_g(\text{gap} < D) = 1 - (1 - P_D)^L \quad (14)$$

with the restriction that $0 < D < U/2$ and

$$P_D = \sum_{m=0}^{\infty} \int_{mU-D}^{mU+D} d\mu' p(\mu - \mu'). \quad (15)$$

With increasing J/U the MI/BG phase border in the J/U - μ/U -diagram remains a random variable, but with a reduced steepness in the slope for finite systems, as shown in^{21,32}. The BG/SF would also be very likely (in a statistical sense) to move to larger critical values of J in a finite system, as the occurrence probability of 'rare events', favoring a SF, is suppressed.

IV. BOX DISORDER

Results for box disorder at $T = 0$ obtained by SMFT have been presented in³⁸, here we extend the phase diagram by taking collective excitation in the BG into account and focus on finite temperature. All numerical results presented in this paper are for a three-dimensional cubic lattice ($Z=6$). Box disorder is characterized by a constant probability density for the on-site energies $p(\epsilon) = \frac{1}{\Delta}\Theta(\Delta/2 - |\epsilon|)$ over a bounded interval of width Δ , where $\Theta(x)$ denotes the Heaviside function. Changing the disorder strength may have an influence on the system properties on various levels. Coming from the insulating state within a local mean-field picture, where the total state of the system is a direct product of local Fock states minimizing the total energy, an increase in disorder reduces the smallest possible particle or hole excitation energy. The local energy gap for a site with an effective chemical potential μ' and a Fock state as ground state $|n = \max([\mu'/U], 0)\rangle$ is $E_{\text{particle}} = \max([\mu'/U], 0)U - \mu'$ for adding a particle and $E_{\text{hole}} = \mu' - (\max([\mu'/U], 0) - 1)U$ for creating a hole, if $\mu' > 0$. In the presence of disorder in an infinitely large system, this implies that the energy gap is necessarily reduced by $\Delta/2$ and vanishes in the $J \rightarrow 0$ limit as soon as the interval of realizable effective chemical potentials contains a positive integer multiple of U , i.e. $\mathbb{N} \cap [(\mu - \Delta/2)/U, (\mu + \Delta/2)/U] \neq \emptyset$.

Within the picture of purely local excitations, this argument is independent of temperature and directly re-

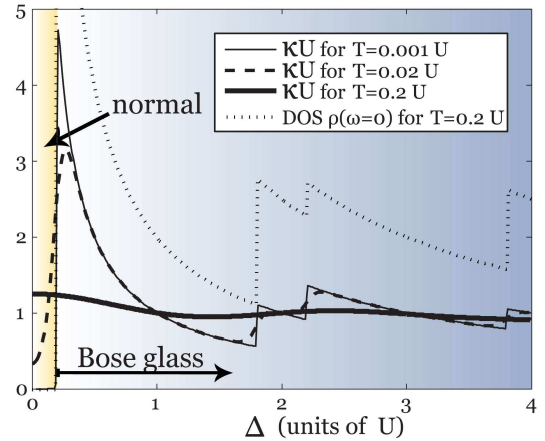


FIG. 2: (Color online) Compressibility κ and local single particle DOS in an insulator for box disorder at $\mu = 1.1U$ at various temperatures (in units of U^{-1}). At zero temperature κ vanishes in the MI, but not in the BG and may thus be taken as a quantity to distinguish between them. At finite temperature however, κ becomes non-zero in the normal phase and the sharp features become rounded off by thermal fluctuations. In this case, the disorder averaged DOS of local excitations $\bar{\rho}(\omega = 0)$, which retains all sharp features at $T > 0$, can be used to determine the crossover from a BG to the normal phase, where it remains zero.

flected by the disorder averaged local DOS

$$\bar{\rho}(\omega, \mu, \Delta, \beta) = \frac{1}{\Delta} \sum_{m=0}^{\infty} (m+1) \frac{\Theta(\frac{\Delta}{2} - |\omega - Um + \mu|)}{Z(Um - \omega)} \times \left[e^{-\beta E_m(Um - \omega)} + e^{-\beta E_{m+1}(Um - \omega)} \right]. \quad (16)$$

In the case of bounded disorder, this directly implies that the system cannot be in a gapped state as soon as the carrier width (Δ for box disorder) equals or exceeds U and that the system is then always in the BG or SF state, i.e. the MI and normal state can only exist at $\Delta < U$ (and not at all for unbounded disorder). When the system is either of these two insulating states at zero temperature, the compressibility $\kappa = \frac{\partial \bar{n}}{\partial \mu}$ is determined by $\bar{\rho}(\omega = 0)$ within a picture of local excitations, where locally degenerate sites change their occupation number by ± 1 if μ is slightly altered. Since for finite temperature thermal particle or hole excitations are also present when the system is gapped, κ is always driven to a finite value. The behavior of κ and $\bar{\rho}(\omega = 0)$ is shown in Fig. 2 at the specific chemical potential of $\mu = 1.1U$. Starting at $\Delta = 0$, the system is in a gapped MI / normal state, but increasing Δ , the system undergoes a phase transition at a critical disorder strength of $\Delta = 0.2U$.

At this point the local DOS $\bar{\rho}(\omega = 0)$ takes on a non-zero value, as two different local Fock states can become degenerate at the edge of the box disorder distribution. At low temperatures the compressibility exhibits a significant change from an exponentially small value in T in the normal phase to a large value due to the existence of local configurations of on-site energies which give rise to almost degenerate states with different particle number. There, a small change in the chemical potential leads to a local jump in particle number. In the zero temperature limit the compressibility locally behaves as $\kappa \propto \frac{1}{\Delta}$, since with increasing disorder strength the statistical weight of these events is reduced. When the effective chemical potentials at the borders of the probability distribution enter a region corresponding to a new local particle number $\mu \pm \frac{\Delta}{2}$, the compressibility increases with a jump, corresponding to subsidiary phase transitions between different BG phases at $T = 0$, which turn into less pronounced crossovers with increasing T . Considering the limit of strong disorder $\Delta/U \rightarrow \infty$ at fixed μ/U in Fig. 2, the system approaches a state in which only half the number of sites are occupied and $\lim_{\Delta \rightarrow \infty} \kappa = \frac{1}{2U}$.

However, disorder does not only affect local excitation properties, but leads to an intricate interplay between the hopping and interaction energy scale, influencing the overall coherence properties of the system. Whereas an increase in temperature or interaction energy generally tends to counteract the formation of a condensate, this is true in most, but not all scenarios when increasing the disorder strength. In certain parameter regimes at sufficiently low temperature, an increase in Δ can actually lead to the formation and stabilization of a condensate

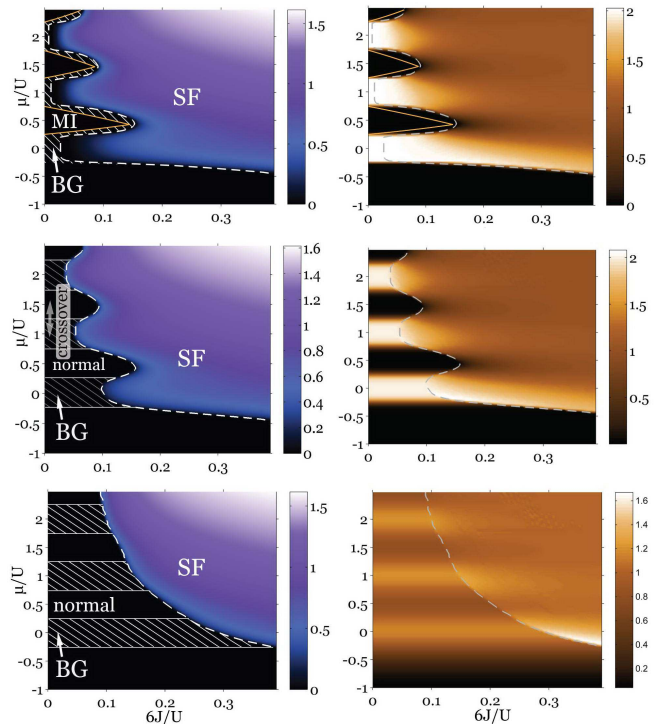


FIG. 3: (Color online) Finite temperature phase diagrams for box disorder with $\Delta = 0.5U$ for three temperature regimes: Zero temperature (upper row), intermediate $T = 0.03U$ (middle row) and high temperature regime $T = 0.2U$ (lower row). The left column shows the expectation value of the self-consistently determined distribution, which is the order parameter for the SF-insulator transition. It vanishes in the MI, BG, and the $T > 0$ normal phase. In the $T = 0$ diagrams, the MI/BG phase borders from strong coupling theory are indicated by the orange solid lines. The BG phase is marked by white stripes, at finite $T > 0$ this is determined by a vanishing local DOS only (i.e. not by strong coupling theory). At finite temperature there is only a crossover between the normal and BG phase, and the borders determined by the DOS of purely local excitations is marked by the horizontal white lines. The right column shows the compressibility κ in units of U^{-1} . Whereas this is a suitable quantity to distinguish the MI (incompressible) from the BG at $T = 0$, it is non-zero, but exponentially small in T in the MI in the intermediate regime and of order U^{-1} in the high temperature regime. The white borders indicate the transition to the SF, determined from the respective diagram on the left.

(i.e. disorder induced condensation), as previously predicted by various methods, including SMFT³⁸.

In Fig. 3, the effect of increasing temperature is exemplified in three phase diagrams and the compressibility in the three main regimes: the zero, low and high temperature regime at fixed disorder strength. The tips of the MI /normal lobes remain almost unchanged under an increase in T , while the BG region between the initial lobes is strongly enhanced and stabilized, even at a very low temperature of $kT = 0.03U$ (central plots of Fig. 3). Since the SF/insulator phase border still possesses a dis-

tinctive lobe structure, but the BG region is strongly enhanced in contrast to the $T=0$ case (upper plots of Fig. 3), we therefore refer to this situation as the intermediate temperature regime. Furthermore, a large value of compressibility is still a strong indicator for the BG at this temperature, suggesting that it may still be useful as an indicator of the transition between the BG and the normal phase in experiment. In the high temperature regime $kT \gtrsim 0.2U$, on the other hand, (see lower diagrams in Fig. 3) the compressibility is large throughout, approaching the value $\kappa \rightarrow U^{-1}$ in the high T limit. The typical temperature of $T \approx 0.2U$ at which the MI and normal phase melts is consistent with previous studies⁴⁴. In this temperature regime the lobe structure of the SF/insulator phase border is totally wiped out and the critical border to the SF follows a $(JZ)_c \propto \mu^{-1}$ decay with increasing filling.

The SF/BG transition is highly sensitive to the system size. When the system approaches the SF phase from the BG phase, the localized single particle orbitals occupied by a large number of bosons increase in size and are occupied by an ever increasing, but never extensive number of particles in the BG phase. At the transition point the localization length, being a measure for the size of these orbitals, diverges and driven by percolation, phase coherence between neighboring orbitals is established, eventually driving the system into the SF phase. In finite size systems, the detection of the transition point thus critically depends on the system size, as the BG phase may be mistaken for the SF phase if the localization length is larger than the system size. SMFT has the advantage that it is constructed in the thermodynamic limit for an infinitely large system in the grand canonical ensemble and takes all possible disorder realizations into account within a functional description for the probability distributions. The numerical error in the discretization performed for the distribution $P(\psi)$ is well controlled and to be distinguished from the finite size deviations made in real space calculations.

In the phase diagram for box disorder Fig. 3, SMFT does not give rise to a direct transition from the MI to the SF, if the extended criterion for the MI/BG border, including collective excitations in rare regions is used. This is furthermore demonstrated in the finite temperature phase diagram at constant filling $n = 1$ in Fig. 4. Due to the absence of a clear distinction between the normal and BG phase at $T > 0$, the orange border only indicates a crossover between these regimes, but would go over into a MI/BG phase border for $T = 0$. At any $\Delta > 0$ a finite BG region intervenes between the MI and SF phases.

The question whether this transition always occurs via the BG phase has been a highly debated topic since the introduction of the disordered BHM¹, and was established for the one and two dimensional case^{22,27,45}. In a recent work²⁴ it was shown that this scenario is true in any finite dimension for bounded disorder, due to the statistical certainty that any possible configuration of on-

site energies for a cluster of sites will occur in the limit of an infinitely large system. In the previous work³⁸ these collective excitations in the BG phase were not considered and within a simpler framework of purely local particle and hole excitations, a direct transition was predicted.

It is known that arithmetically averaged MFT, as well as SMFT providing an improvement in any finite dimension, both become exact in the limit of infinite dimensions, where no BG exists at $T = 0$. However, as argued recently²⁴ the theorem of inclusions guarantees the existence of an intervening BG phase between the SF and the MI in any arbitrarily high, but finite number of dimensions for bounded disorder. It is instructive to understand the decrease of the BG region, including the collective excitation in the Lifshitz regions in terms of percolation physics: For any finite dimension the outer border between the BG and SF phase specifies the critical value $(J/U)_{\text{crit.1}}$ specifies the lowest energy at which it becomes energetically favorable for the particles to form a global condensate (in SMFT this is the border where $\bar{\psi}$ takes on a finite value). The border between the MI and BG inside the global insulator, specifies the critical value $(J/U)_{\text{crit.2}}$ at which it becomes possible for the system to form large local superfluid patches (locally resembling pure systems) without phase coherence between different patches. With increasing dimensionality of the system, the connectivity between different patches increases (percolation is enhanced) and the required tunneling energy $(J/U)_{\text{crit.1}}$ to form one large percolated patch, i.e. a global condensate, decreases. In the limit of high dimensions, the critical values of J at which these two phenomena occur approach the arithmetically averaged mean-field value³⁷

$$JZ_c(\mu) = \Delta \left[n \ln \left(\frac{1 - n + \mu + \Delta/2}{1 - n + \mu - \Delta/2} \right) + (n + 1) \ln \left(\frac{n - \mu + \Delta/2}{n - \mu - \Delta/2} \right) \right]^{-1}, \quad (17)$$

and the BG disappears, where n is the filling and μ and Δ are given in units of U .

In Fig. 4 we present a phase diagram calculated at fixed density $n = 1$ in the low temperature regime $T = 0.03U$. At every point in the diagram, the self-consistent distribution is calculated for a fixed μ , enabling the calculation of the density $\langle n(\mu, \Delta, U, J, T) \rangle$. Thereafter μ is iteratively determined using Ridder's algorithm⁴⁶ until the density obtained from SMFT does not deviate more than $\Delta n = 0.005$ from the specified density. In Fig. 4, the disorder averaged MFP $\bar{\psi} = \int \psi P(\psi) d\psi$ (within SMFT, this is exactly $\sqrt{f_c n}$) clearly shows the usual SF/insulator phase transition (at fixed low temperature) along the line $\Delta = 0$, where the disorder localizes the particles with increasing U/J . Moving outwards into the Δ/J at fixed interaction U/J , the condensed phase is surprisingly robust, surviving local on-site fluctuations Δ several hundred times larger than the hopping energy J , as pointed out in a recent work²⁵. This can be understood from

the bosons filling up the low-lying sites and forming a 'background sea' via the repulsive interactions, creating an effective smoother potential in which it is energetically favorable for the remaining bosons to delocalize³⁸. A remarkable effect at sufficiently low temperature is the appearance of a SF lobe, protruding into the insulating domain at finite Δ . In this regime the interplay between disorder and interactions is non-monotonic in these two effects, and, for the regime $40 \lesssim U/J \lesssim 85$, an increase in Δ drives the system into the SF phase, delocalizing the particles. This effect can be understood from the pure BHM μ/U - J/U phase diagram and relies on the existence of a lobe structure, i.e. requires a sufficiently low T . To keep the particle number constant with increasing Δ , μ is required to increase. In certain regimes the majority of sites in the system may enter from an insulating regime between the lobes into a regime inside the lobes, thereby favoring condensation. Qualitatively, the SMFT phase diagram agrees well and shows the disorder induced SF lobe, as found in recent QMC calculation²⁵ at $T = 0$ on relatively small lattices ($L = 8 \times 8 \times 8$).

At large Δ the order parameter is non-monotonic in U/J , vanishing at sufficiently small U/J which indicates a transition into an Anderson localized state, where the localization almost exclusively disorder-induced. However, the region of extremely small U/J is problematic

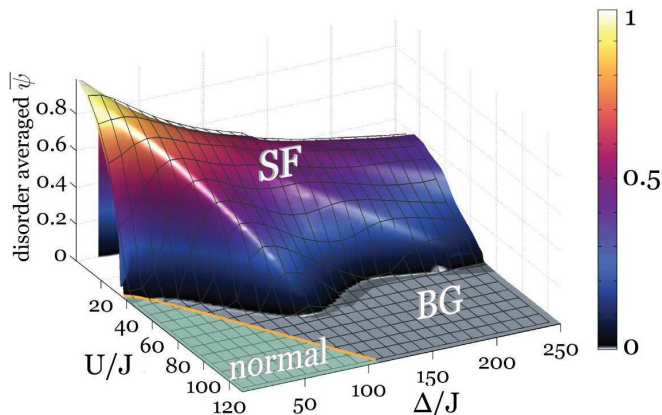


FIG. 4: (Color online) Phase diagram for box disorder at fixed density $n = 1$ in the U/J - Δ/J plane at $T = 0.03U$ showing the mean order parameter $\bar{\psi} = \sqrt{f_c}$. Reentrant superfluidity is reflected by the protruding SF lobe (we also find a second less pronounced lobe at higher Δ), where increasing Δ can drive the system through a sequence of SF-insulator transitions. The orange line specifies the crossover from the normal to the BG phase (at $T = 0$ this line becomes the MI-BG phase border) as determined by by shifted mean-field phase borders at this temperature, giving a better approximation than the strong-coupling approach for three dimensions. The simpler criterion of looking at purely local particle and hole excitations Eq. 16 would lead to the MI/BG phase border at $U = \Delta$ and predict a direct MI-SF transition at small Δ . Including collective excitations in the BG, as done here, always leads to an intermediate BG phase between the MI and SF in the $T = 0$ limit.

as Δ/U and μ/U diverge, since very few sites have to contain an ever increasing number of particles to keep the disorder-averaged density fixed, when asymptotically half the number sites (due to the symmetry of the box distribution $p(\epsilon)$) have such a high effective on-site energy, that they contain no particle. Due to the diverging local occupation number, this limit transcends the constraints imposed in the derivation of the BHM in an optical lattice and is, in this sense, unphysical.

V. SPECKLE DISORDER

Although a homogeneous box distribution is most commonly used for disorder calculations in theory, it is currently not an experimentally feasible choice. In this section we discuss and compare the results for a realistic disorder distribution created by a speckle laser to those of a box disorder distribution. A laser passing through an inhomogeneous disordered plate leads to a disordered optical potential, which is the Fourier transform of the disordered pattern on the plate. In recent experiments, it has become possible to reduce the autocorrelation length of this disordered potential to the order of the lattice spacing ($\leq 1\mu m$)¹⁶. With this experimental achievement, the priorly most criticized artifact of a speckle laser for creating uncorrelated disorder has been overcome, thereby making speckle potentials the most promising method for future disorder experiments in optical lattices. The resulting distribution for uncorrelated on-site energies is well approximated by

$$p(\epsilon) = \frac{\Theta(\epsilon)}{\Delta} e^{-\epsilon/\Delta} \quad (18)$$

Although it may be argued that an optical speckle potential in experiment is fundamentally bounded by its finite size, it is only essential that the width of the on-site energy distribution exceeds U (which is fulfilled in essentially all experimentally relevant regimes). This justifies the use of (18).

To treat this disorder distribution using SMFT, it is useful to perform a transformation of variables $x(\epsilon) = -e^{-\epsilon/\Delta}$, which on a formal level transforms the SMFT conditional probability functions into a form analogous to homogeneous disorder. This step enters only on the level of calculating the conditional cumulative distribution function (CDF),

$$F(\psi|\eta) = \lim_{c \rightarrow 0} \int_{c-1}^0 dx \Theta(\psi - g(\mu + \Delta \ln(-x), \eta)). \quad (19)$$

Apart from this, the SMFT method remains identical to the homogeneous disorder case. Similarly, arbitrary disorder distributions may also be incorporated into SMFT, although an analytical transformation of the random variable will not exist in general.

In contrast to box disorder, which has been the distribution primarily focused on so far when considering

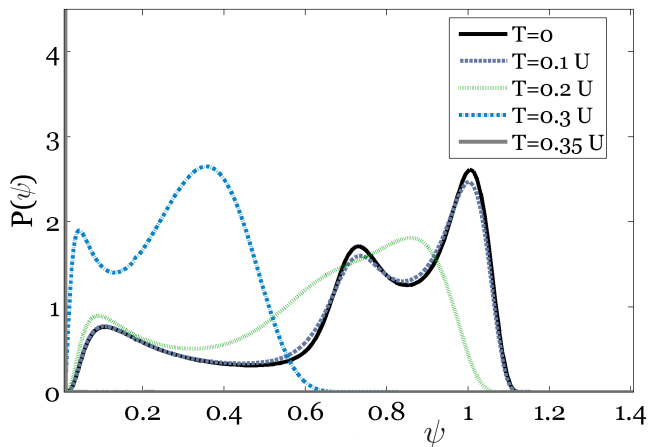


FIG. 5: (Color online) Typical self-consistent distributions $P(\psi)$ for speckle disorder for $\Delta = 1U$, $\mu = 1.2U$, $Z = 6$, and $JZ = 0.3U$ at different temperatures. For low temperatures the mean-field parameters in the condensed phase are robust against finite temperature fluctuations, but with increasing temperature the system is eventually driven into an insulating BG phase, as indicated by the distribution at $P(\psi) = \delta(\psi)$ in the at $T = 0.35U$.

the disordered BHM, speckle disorder is unbounded and arbitrarily high values of ϵ have a finite probability to occur. This leads to the effect (strictly only possible for an infinitely large system) that *turning on* the disorder by an arbitrarily small amount immediately changes a large part of the phase diagram from the MI / normal phase into the BG phase.

In a physical picture, the effective chemical potential μ' can then take on integer multiple values of U (the on-site potential can become arbitrarily high) with a non-zero probability density, where local Fock states with different particle number become degenerate, leading to a finite compressibility and local DOS $\bar{\rho}(\omega = 0)$ at $T = 0$.

In the absence of disorder and at sufficiently high tunneling coupling J , a macroscopic number of particles occupy the $|k = 0\rangle$ Bloch state. Within an effective, symmetry breaking Gutzwiller description the local order parameters $\psi_l = \langle b \rangle_l$ then take on a finite and constant value, reflecting the translational symmetry of the system. Within SMFT this state is characterized by a δ -distribution $P(\psi) = \delta(\psi - \psi_0)$, where ψ_0 is the order parameter of conventional bosonic Gutzwiller theory. Turning on the disorder in such a system in the SF state breaks the translational symmetry of the system, i.e. the condensate state deviates from the $k = 0$ Bloch state, which is reflected by the distribution of MFPs $P(\psi)$ taking on a finite width. Initially for weak disorder, an increase in disorder always leads to a broadening of $P(\psi)$, but for stronger values of Δ the system may eventually be driven toward an insulating state, driving $P(\psi) \rightarrow \delta(\psi)$ and thereby decreasing the fluctuations in the MFPs. On the other hand, increasing the temperature suppresses the SF and leads to a decrease of the MFPs above a cer-

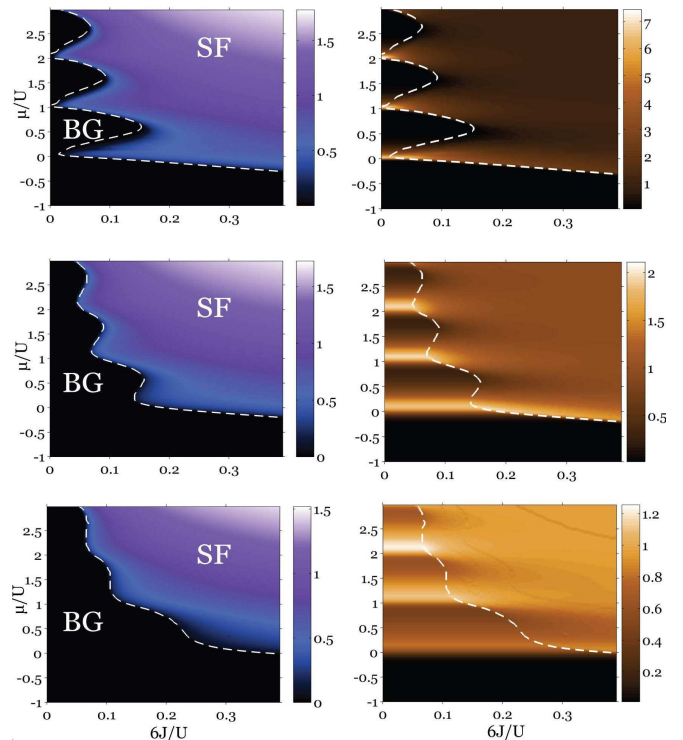


FIG. 6: (Color online) Disorder averaged MFP $\bar{\psi} = \int d\psi \psi P(\psi)$ characterizing the SF-insulator transition (left column), and compressibility (right column, in units of U^{-1}) in the $JZ/U - \mu/U$ -plane for *speckle disorder*. Diagrams are shown for increasing disorder strength ($\Delta = 0.1U$, $\Delta = 0.3U$, $\Delta = 1U$) in the zero or low temperature regime ($T = 0$, $T = 0.05U$, $T = 0.05U$) for the (upper, middle, lower) row respectively. In contrast to the behavior for box disorder, the structure of each lobe does not change symmetrically, but rapidly extends in the direction of decreasing μ/U with increasing disorder strength Δ . Since the MI / normal phases do not exist for speckle disorder, the insulating region (black in the left figures) is always a BG. The white lines denote the SF / insulator phase boundaries, indicating where $\bar{\psi}$ takes on a finite value.

tain temperature, up to which the SF remains stable, as shown in Fig. 5.

The influence which speckle disorder has on the $\mu/U - J/U$ -phase diagrams is shown in Fig. 6. In contrast to box disorder, where the distribution of on-site energies is symmetric around μ and the insulating lobes give way to the SF in the same way on the upper and the lower side of the lobe, the insulator forms on the lower side of the lobes with increasing Δ for speckle disorder. This can be understood from the fact that only lower values of the effective local chemical potential can occur.

For strong disorder $\Delta \gtrsim U$, the lobe structure of the insulator / SF phase boundary is washed out, which is similar to the effect of finite temperature. For speckle disorder, κ cannot be used to identify a phase transition, since it is non-zero in both the BG and the SF. A question of interest, regarding the disappearance of the MI

/normal phase for an arbitrarily small amount of speckle disorder, is how the compressibility behaves as a function of Δ , as some interpretation is needed, that an 'infinitesimal amount of disorder' can instantaneously convert the whole MI/normal area of the phase diagram into a BG.

In Fig. 7, $\kappa(\Delta)$ is shown for different parameters to clarify this dependence. In the insulating state, the compressibility can be calculated explicitly (D3) and one obtains

$$\kappa = \frac{1}{\Delta} \left[\frac{\sum_m m e^{-\beta E_m(\mu)}}{\sum_m e^{-\beta E_m(\mu)}} - \frac{1}{\Delta} \int_0^\infty d\epsilon e^{-\frac{\epsilon}{\Delta}} \frac{\sum_m m e^{-\beta E_m(\mu-\epsilon)}}{\sum_m e^{-\beta E_m(\mu-\epsilon)}} \right] \quad (20)$$

Essentially, two different scenarios have to be considered. First, if μ/U is positive and integer, κ diverges in the limit of vanishing disorder, as is well known from the pure BHM phase diagram, where the density is a step function in μ/U for $J = 0$. This is equivalent to the

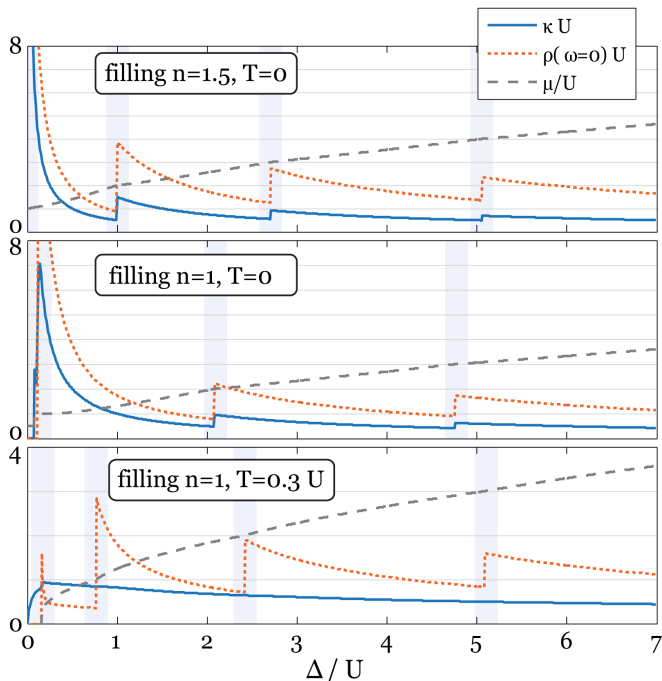


FIG. 7: (Color online) The compressibility, local single particle DOS and chemical potential as a function of disorder strength Δ for speckle disorder at constant filling. Comparison of the upper two plots shows a diverging compressibility and local DOS for $\Delta \rightarrow 0$ for non-integer filling (the system remains superfluid), while for integer filling it drops to an exponentially small value in Δ at a value of $\Delta \approx 0.1U$ and vanishes in this limit. The lowest figure shows the same quantities at finite temperature $kT = 0.3U$, where thermal fluctuations have totally smeared out the sharp features in the compressibility. However, these persist in the local DOS, although their position is changed due to a temperature induced shift in μ .

case for non-integer, fixed particle density n , where the system remains SF for any non-zero J . Second, if μ/U is non-integer, the compressibility vanishes with decreasing Δ , as the system approaches a point in a Mott lobe away from the border. This corresponds to the case of fixed, integer-valued density n .

We will now discuss the behavior of κ and $\bar{\rho}(\omega = 0)$ at fixed particle density n , shown in Fig. 7. Keeping the density constant with rising disorder, requires the chemical potential to be increased, as an ever increasing number of sites shifts to weights with lower occupation numbers. At every point when μ/U passes a positive integer number, a new Fock state becomes potentially occupied, but with an ever decreasing statistical weight as Δ increases. As a result the compressibility experiences a jump at each of these points, as highlighted by the gray regions in Fig. 7, where μ/U (dotted gray lines in Fig. 7) passes an integer value. This leads to the characteristic series of ever smaller kinks in $\kappa(\Delta)$. At finite temperature, these features in κ are smeared out over a typical scale of kT , whereas the sharp features in the local single particle DOS survive at $T > 0$ within SMFT (solid blue lines in Fig. 7).

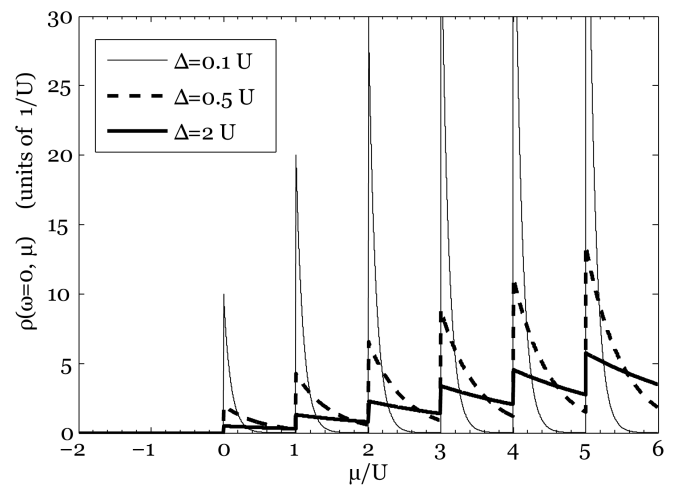


FIG. 8: The disorder averaged single particle density of states $\rho(\omega = 0, \mu)$ at zero frequency for $T = 0.05U$ for different speckle disorder intensities. For $\Delta = 0$ this consists of a sequence of δ -peaks at positive integer values of μ/U , however for any $\Delta > 0$ this quantity is non-zero for $\mu \geq 0$ and the system is in the BG phase.

To clarify the effect speckle disorder has on $\bar{\rho}(\omega = 0)$ and the immediate disappearance of the MI / normal phase at any $\Delta > 0$, the local DOS is plotted for weak ($\Delta = 0.1U$), intermediate ($\Delta = 0.5U$) and strong ($\Delta = 2U$) in Fig. 8 as a function of μ . In the pure system $\bar{\rho}(\omega = 0, \mu)$ consists of a sum of δ -peaks at integer values of μ/U , i.e. at these values of the chemical potential there are two degenerate Fock states $|n = \mu/U\rangle$ and $|n = \mu/U + 1\rangle$ at all sites in the insulator and the local single particle DOS diverges. As soon as speckle disorder is turned on, these δ -peaks are broadened according to

the on-site energy distribution (18) and $\bar{\rho}(\omega = 0)$ takes on the form of a sequence of superimposed exponential functions, each decaying with the constant Δ . From this it is clear that $\bar{\rho}(\omega = 0)$ takes on a non-zero value as soon as $\Delta > 0$ at any $\mu > 0$, although it is exponentially suppressed for most values of μ at weak disorder $\Delta \ll U$. At zero temperature the different amplitudes of the various peaks in $\bar{\rho}(\omega = 0, \mu)$ at integer μ can be exclusively attributed to the \sqrt{n} factor from the action of the bosonic operators, whereas at $T > 0$ the amplitudes (but not the positions of the sharp features) may also be modified by the Boltzmann factors in (E4).

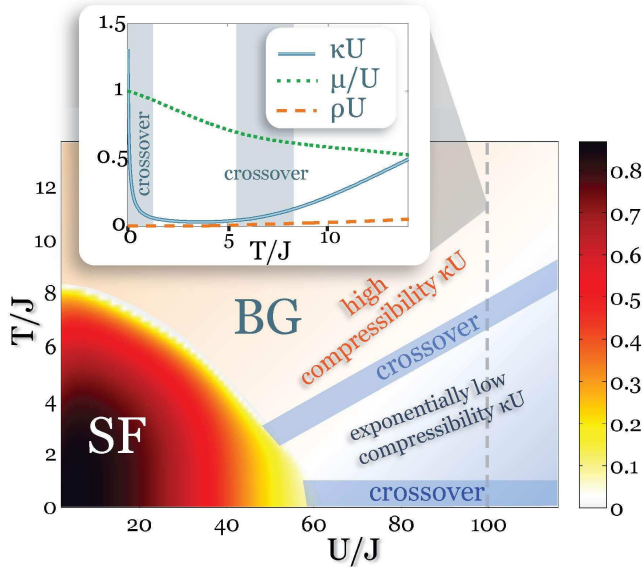


FIG. 9: (Color online) Main image: Phase diagram in the T/J - U/J -plane for fixed $\Delta = 10J$ at fixed filling $n = 1$ in three dimensions. For this specific disorder strength the SF region is enlarged by the disorder in comparison to the pure case (i.e. disorder induced condensation, see Sec. V A). In the lower left corner, the SF exists at sufficiently low T and Δ and the value of disorder-averaged $\bar{\psi}$ is color-coded. Outside the SF region, the system is always in a BG phase, but undergoes two crossovers from a regime with exponentially low compressibility κU for intermediately low $0.02 \lesssim T/U \lesssim 0.065$ (for $\Delta/J = 10$) into a strongly compressible BG regime, in the limits of both high and very low T/U . To clarify the quantitative behavior, the compressibility κ , the chemical potential μ and the local single particle DOS $\rho(\omega = 0)$ along the dashed line $U/J = 100$ is shown in the inset.

Fig. 9 shows the phase diagram at constant disorder strength $\Delta/J = 1$ and constant density $n = 1$ in units of J . The SF region prevails in the lower left region at low temperature and weak interaction U/J . In this parameter regime the disorder stabilizes the SF phase, actually extending the SF region of the phase diagram in contrast to the pure ($\Delta = 0$) case (disorder-induced condensation, see Sec. V A). All of the non-SF region in Fig. 9 is a BG, since we are dealing with unbounded disorder with $\Delta > 0$, but we can identify a weakly and

two strongly compressible regimes in the phase diagram. Since $P(\psi) = \delta(\psi)$ in the BG, the energy scale J cannot influence thermodynamic quantities beyond a scaling relation, implying that the compressibility κU may be a function of T/U only. Therefore the compressibility has a radial structure and it suffices to consider its behavior along a single line (such as $U/J = 100$, depicted in the inset of Fig. 9). This reveals that there are three regimes in this phase diagram: at high temperature $T/U \gtrsim 0.065$ the system is strongly compressible (κU is of order unity), as thermal fluctuations have wiped out the sharp peaks over a wide range in μ . At intermediately low temperature, the compressibility is exponentially low, as the typical thermal excitation energy scale does not suffice to excite the majority of sites to higher states. Somewhat surprisingly, within a certain parameter regime for Δ and the density n , the system undergoes a further crossover at very low temperature $T/U \approx 0.02$ into a second highly compressible regime. At $T = 0$ and at integer filling, the chemical potential μ/U approaches an integer value from below (green dotted line in the inset of Fig. 9). At these points κ diverges in the pure limit of $\Delta \rightarrow 0$, which reveals that the compressibility grows with the inverse of Δ and only persists in the limit $T \rightarrow 0$ if the density n is integer.

A. Disorder-induced reentrant Superfluidity

At low temperature and fixed density, we find that an increase in Δ can actually drive the system from an insulating into a condensed state within a certain window of U/J , as shown in Fig. 10 and Fig. 11. Within a very small window of U/J , the system may be driven through an additional sequence of BG and SF phases.

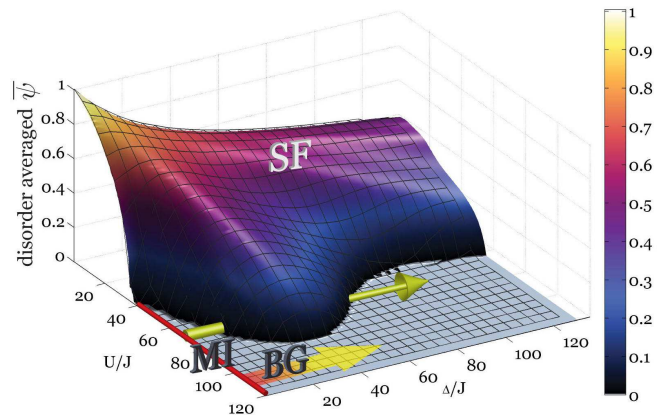


FIG. 10: (Color online) Low temperature $kT = 0.03U$ phase diagram showing the disorder-averaged MFP $\bar{\psi}$ for speckle disorder at constant filling $n = 1$ in three dimensions. Multiple reentrant behavior can be seen within a small window of U/J . The red line at $\Delta = 0$ indicates the presence of MI / normal state, for any $\Delta > 0$ the insulator is a BG.

On the $\Delta = 0$ line, the usual SF - insulator transition

occurs, whereas along Δ for small values of U , disorder only suppresses the SF slightly up to reasonably large values of Δ/J . For even larger disorder values, the system will eventually undergo the transition into an

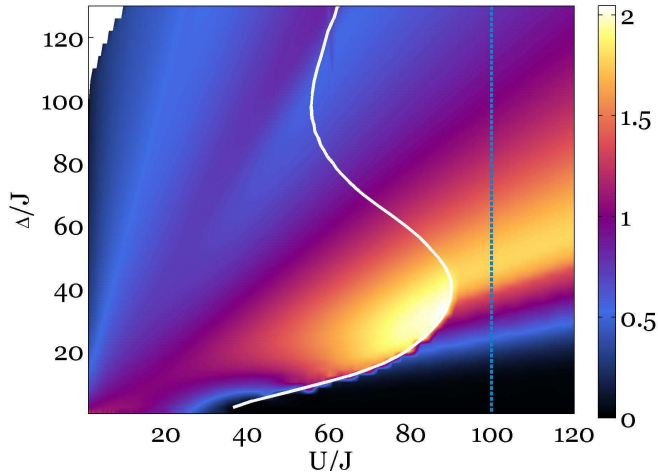


FIG. 11: (Color online) Compressibility κ in units of $1/U$ at $kT = 0.03U$ for speckle disorder at constant filling $n = 1$ in three dimensions (same parameters as in Fig. 10). The incompressible normal phase only exists on the line $\Delta/J = 0$, but the region where κ is exponentially small in the insulator extends linearly with U/J . The white line is the SF - insulator phase border, where $\bar{\psi}$ becomes zero. The compressibility along the blue dashed line can be understood as the low temperature case and compared to κ in the lower two plots of Fig. 7, where the sharp features have been washed out by temperature, but are still pronounced peaks.

Anderson localized state. In comparison to the corresponding phase diagram for box disorder Fig. 4, the extruding superfluid lobe appears at a considerably smaller values of $\Delta \approx 40J$ for speckle disorder ($\Delta \approx 100J$ for box disorder, not the different Δ -axis scale). However, it should be noted that the measure Δ is not the same (in a statistical sense) for the two disorder types: whereas for speckle disorder Δ is also the standard deviation (std), in the case of box disorder the std is only $\frac{\Delta}{2\sqrt{3}} \approx 0.29\Delta$, corresponding to weaker disorder for the same Δ . Examining the position of the superfluid lobe in units of the standard deviation, actually reveals that it appears at slightly smaller disorder strengths for box disorder.

In the vicinity of the phase border, κ is generally larger in the SF state than in the neighboring insulator, as a shift in μ leads to a locally continuous shift in density. On the lower side of the lobe at disorder strengths $\Delta \lesssim 40J$, the compressibility jumps across the phase border (i.e. second order transition). At higher values of Δ , κ is almost unaffected by the disappearance of the condensate, i.e. the compressibility is almost exclusively induced by disorder. In the insulating state the ensemble of mean-field states determined by SMFT cannot depend on J (since different sites are only coupled via ψ). Therefore any physical quantity, such as κ , can only be a function

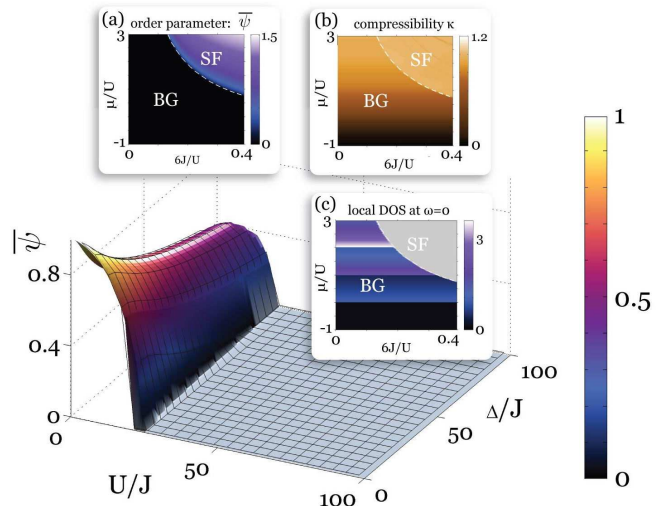


FIG. 12: (Color online) Main background image: same $\bar{\psi}$ phase diagram as in Fig. 10, but in the experimentally relevant high temperature regime $kT = 0.3U$ at $n = 1$, where disorder cannot induce condensation. Insets: disorder averaged MFP (a), compressibility (b) and local DOS $\bar{\rho}(\omega = 0)$ in the $\mu/U - JZ/U$ -plane at the same temperature $T = 0.3U$ for $\Delta = 1U$. In this regime most interesting structure has been washed out by thermal fluctuations and disorder and an increase in either U , Δ or T *always* suppresses condensation.

of T/U in this regime (reflected in the radial structure of κ in the insulator).

In the high temperature regime relevant for current experiments (see App. VIA for an approximation of T), the lobe in the $\Delta/J - U/J$ -plane at fixed density has vanished completely and an increase in disorder always counteracts the condensate formation. This might explain the recent finding, that no reentrant behavior or disorder-induced condensation was observed in experiments so far¹⁷. Furthermore, we calculated the $\mu/U - J/U$ -phase diagram for this temperature and disorder regime, where the lobe structure is also fully washed out and the system is dominated by thermal fluctuations, as seen in the insets of Fig. 12. We therefore conclude that an upper critical temperature, which may depend on the filling, exists for the occurrence of reentrant superfluidity. Our temperature estimation suggests that T is too high in current experiments to observe this effect, which agrees with recent experimental evidence¹⁷.

B. Hopping Disorder

In addition to diagonal on-site energy disorder, it is possible to incorporate off-diagonal hopping disorder⁴⁷ into the SMFT formalism. In this case, the local hopping energy $J_{\langle i,j \rangle}$ between site i and j becomes a random variable, each described by a distribution $p_J(J)$, which we assume to be independent of the on-site energies ϵ_i .

This leads to the BH Hamiltonian with on-site, as well as hopping disorder

$$\begin{aligned} \mathcal{H}_{\text{BH}} = & - \sum_{\langle i,j \rangle} J_{\langle i,j \rangle} (b_i^\dagger b_j + \text{h.c.}) \\ & + \sum_i (\epsilon_i - \mu) n_i + \frac{U}{2} \sum_i n_i (n_i - 1). \end{aligned} \quad (21)$$

The PDF $p_J(J)$ has been calculated for a speckle disorder potential^{16,48} using imaginary time evolution.

In contrast to diagonal disorder (on-site energy or interaction), where the fluctuations are incorporated into the conditional PDF (8) before the iteration procedure of the SMFT self-consistency equations, the hopping disorder acts as an additional source of fluctuations during this iteration procedure, methodically entering at a different point in the method. The corresponding mean-field Hamiltonian $\mathcal{H}_i^{(\text{MF})}$, (analogous to (2)) now depends on the rest of the system only through the new random variable

$$\eta = \sum_{j=1}^Z J_j \psi_j, \quad (22)$$

where both J_j and ψ_j are random variables, the latter again being assumed to be distributed according to $P(\psi)$. It is therefore convenient to introduce the an intermediate random variable $\phi = J\psi$, distributed according to the PDF $P_\phi(\phi)$. As explained in App. C, this new PDF can be expressed explicitly in terms of the PDF's $P(\psi)$ and $p_J(J)$ as

$$P_\phi(\phi) = \int dx p_J(e^x) P(\phi \cdot e^{-x}), \quad (23)$$

numerically allowing the use of the FFT algorithm on a suitable grid. Once $P_\phi(\phi)$ is known, the PDF for the random variable $\eta = \sum_{l=1}^Z \phi_l$ can subsequently be calculated by

$$Q(\eta) = \frac{1}{2\pi} \int dt [\vartheta(t)]^Z e^{-it\eta}, \quad (24)$$

where

$$\vartheta(t) = \int d\phi P_\phi(\phi) e^{it\phi}. \quad (25)$$

is the characteristic function of $P_\phi(\phi)$. For the numerical computation of the previous two, the FFT algorithm can be used.

The conditional PDF (8) $\tilde{P}(\psi|\eta)$, incorporating the effect of any diagonal (here: on-site) disorder remains unchanged under the inclusion of hopping disorder and is calculated before the SMFT iteration procedure in full analogy to the previous case for the relevant on-site disorder type $p(\epsilon)$. The final self-consistency equation, closing the iteration procedure is also left unchanged to the previous case (9)

$$P(\psi) = \int d\eta Q(\eta) \tilde{P}(\psi|\eta), \quad (26)$$

except that the $Q(\eta)$ entering is calculated from (24).

Of course the case of pure on-site disorder with a constant hopping energy J_0 can be obtained as a limit of this extension by setting $p_J(J) = \delta(J - J_0)$, causing (23) and (24) to reduce to (4).

The numerical iteration procedure is carried out analogously to Sec. II A, except that only a single equidistant grid, as restricted by (23), can be used. This limits the numerically obtained precision of $P(\psi)$ at small values of ψ .

In our calculation we use the appropriately scaled distribution $p_J(J)$, matching the on-site disorder strength, as obtained by Zhou and Ceperley⁴⁸ for a lattice depth of $s = 14E_R$ and at a speckle disorder strength of $s_D = 1E_R$, where we assume that the standard deviation in $p_J(J)$ is proportional to the disorder intensity s_D (as motivated by their analysis). Since a change in the disorder strength does not change the most probable value of the distribution⁴⁸ $p_J(J)$, we model the hopping disorder distribution to have its most likely value at the given value \bar{J}/U , with the width being independent thereof. If any weight lies at values of negative J , this is set to zero and the distribution is subsequently renormalized, however this is only relevant for points deep in the insulator and does therefore not influence the results in any way. However, this only occurs at very small values of \bar{J}/U deep in the insulator, making this formal alteration of $p_J(J)$ irrelevant to the result.

As shown in the low temperature phase diagram in the J/U - μ/U -plane (Fig.13), the additional inclusion of hopping disorder leads to a stabilization of the SF phase and a small shift in the phase boundary. For disorder distributions in the typical experimentally relevant parameter regime, the standard deviation of the hopping parameter distribution $p_J(J)$ is three orders of magnitude smaller than the standard deviation of the on-site energy distribution $p(\epsilon)$ (as found in⁴⁸, specifically for the distributions used here $\sigma_J/\sigma_\epsilon = 0.0014$). This explains the minor, but clearly resolved modification of the phase boundaries in contrast to the pure on-site disordered case, shown in the upper right inset of Fig. 13.

VI. INCORPORATING EXPERIMENTAL ASPECTS

A. Temperature estimation in an optical lattice

The initial temperature in the trap, prior to the optical lattice ramp-up, can be determined from the expansion profile of the cloud. If the ramp-up of the optical lattice is performed adiabatically, the entropy of the system is conserved and can actually lead to a cooling of the atoms. The initial entropy of a weakly interacting cloud in the trap using Bogoliubov theory leads to the expression⁴⁹

$$S_{\text{Bog.}}(\beta) = k_B \sum_{\mathbf{p}} \left(\frac{\beta \epsilon_{\mathbf{p}}}{e^{\beta \epsilon_{\mathbf{p}}} - 1} - \ln[1 - e^{\beta \epsilon_{\mathbf{p}}}] \right). \quad (27)$$

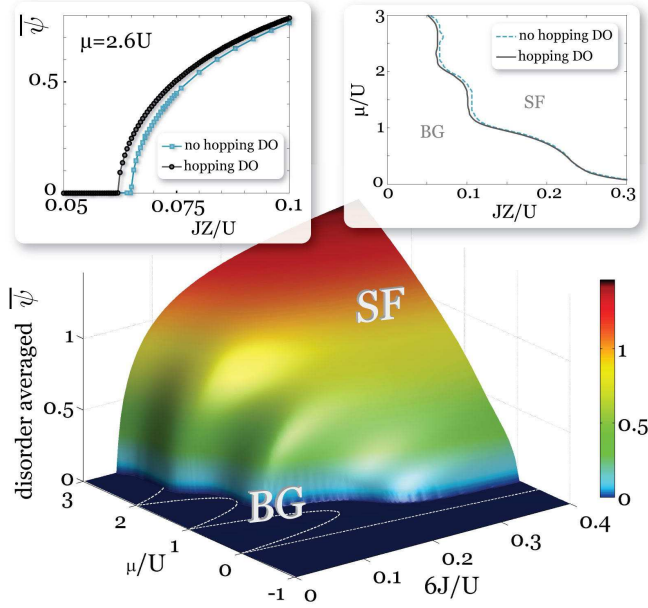


FIG. 13: (Color online) Diagrams showing the effect of *hopping disorder* at $T = 0.05U$ and an on-site speckle disorder strength $\Delta = U$. Main 3D figure: disorder-averaged MFP ψ for speckle on-site and experimentally corresponding hopping disorder. For orientation purposes, the MF phase boundary for the pure system is plotted as a thin dashed white line. The value J/U refers to the most likely value of the hopping disorder distribution $p_J(J)$, whereas the width of the distribution $p_J(J)$ is constant. Upper left inset: comparison of the order parameter at fixed $\mu = 2.6U$ with and without hopping disorder, clearly demonstrating that the addition of hopping disorder stabilizes the SF phase and leads to a lower critical value of J in this regime. Upper right inset: Subsequent comparison of phase borders in the μ/U - J/U -plane.

After ramping the lattice to a sufficiently high intensity, the entropy can be calculate up to first order (neglecting terms containing J)⁴⁹

$$S_{J=0} = k_B \left[-\beta\mu + \frac{1}{N} \ln(\Xi(M)) + \beta E \right], \quad (28)$$

where M is the number of sites and $\Xi(M)$ is the grand canonical partition function. Equating these two expressions for a sufficiently high initial temperature $k_B T_{\text{initial}} > 0.05E_R$ leads to the relation⁴⁹

$$k_B T_{\text{final}} \approx \frac{U}{3E_R} (k_B T_{\text{initial}} + 0.177E_R) \quad (29)$$

For ^{87}Rb in an optical with a wave length of $\lambda = 812\text{nm}$ and intensity $s = 11E_R$, the disorder-averaged interaction constant is $\bar{U}/E_R = 0.355$. As a typical, conservative estimate of the initial temperature before the lattice ramp-up in current experiments⁵⁰ we use the value $T_{\text{initial}} = 0.13\mu\text{K}$, for which the relation (29) predicts a final temperature of $k_B T \approx 0.11E_R = 0.32U$ after the ramp-up.

B. LDA incorporating trap effects

To compare the results obtained via SMFT to experimental data on a quantitative level, we performed a LDA+SMFT calculation to incorporate the effect of the trapping potential. Two effects of the lattice laser beams are taken into account: The red-shifted lattice laser beam with a Gaussian profile and beam width w_0 leads to an attractive potential via the ac Stark effect. Furthermore, the local energies of states within a localized Wannier basis are also increased in regions of high intensity, leading to the renormalized effective lower trapping frequency within an harmonic approximation⁵¹.

$$\omega_{\text{eff}}^2 = \frac{4E_R}{mw_0^2} (2s - \sqrt{s}). \quad (30)$$

With the addition of an external magnetic trap with trapping frequency ω_{mag} , the total trapping frequency, which the atoms are exposed to is given by

$$\omega_{\text{tot}} = \sqrt{\omega_{\text{eff}}^2 + \omega_{\text{mag}}^2}. \quad (31)$$

For every fixed value of the lattice height s , J and U are extracted from the single particle Wannier function (beyond the approximation for deep lattices⁵¹), the total trapping frequency (31) is calculated and the local effective trap energies are assigned on a sufficiently large 3D lattice. The chemical potential μ is adjusted using Ridder's method⁴⁶ to obtain a specified total particle number. The condensate fraction, depicted in Fig. 14, is subsequently averaged over the local values obtained by SMFT, weighted by the respective density.

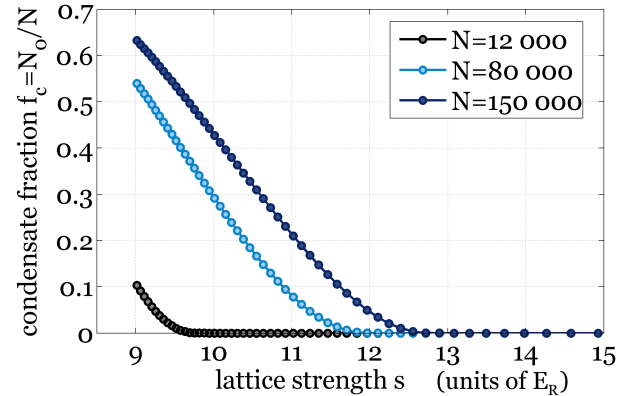


FIG. 14: (Color online) The condensate fraction as a function of the lattice strength s for various total particle numbers in a harmonic trap, calculated within LDA and SMFT (connected dotted lines). The calculations were performed at fixed temperature $kT = 0.3U$ and disorder strength $\Delta = 1U$.

We used the following values for the experimental parameters: $w_0 = 110\mu\text{m}$, the lattice laser wavelength was

set to $\lambda_{\text{lat}} = 812nm$, and the magnetic trapping frequency $\omega_{\text{mag}} = 2\pi 40Hz$.

In contrast to the behavior of the order parameter at the transition point, the condensate fraction does not follow a power law decay in the finite trap, but is smeared out a the transition point, as superfluid regions in the trap decay in size with increasing s .

VII. CONCLUSION

We have described the stochastic mean-field theory in detail on a methodological level, and extend it to incorporate finite temperature effects. Subsequently, we have applied it to ultracold atoms in an optical lattice with uncorrelated on-site box disorder distribution and discussed the intricate interplay between interaction, tunneling energy, disorder, filling and finite temperature effects. Furthermore, we have presented, to the best of our knowledge, the first quantitative theoretical calculations for speckle disorder, which leads to a qualitatively different phase diagram than for box disorder and are of immediate experimental relevance¹⁷. For this case, we have discussed the characteristic features of the various phases and presented phase diagrams, both at fixed chemical potential and at fixed density. Below a critical temperature, we find disorder-induced condensation and multiple reentrant behavior, both for box and speckle disorder. The temperature in recent experiments¹⁷ is estimated and found to be too high yet to observe disorder-induced condensation. We also find that including hopping disorder in addition to local on-site disorder for a realistic distribution of speckle parameters enhances the insulator and jumps in the order parameter within the SF phase indicate a series of transitions. An LDA+SMFT calculation has been performed to incorporate the effects of an external trap for on-site speckle disorder.

Acknowledgments

We thank I. Bloch, L. Carr, B. DeMarco, E. Demler, A. Pelster, D. Semmler, M. Snoek, H. Stoof and W. Zwerger for useful discussions. This work was supported by the German Science Foundation (DFG) via Forschergruppe FOR 801. UB and RT acknowledge support by the Studienstiftung des deutschen Volkes. Calculations were performed at the Center for Scientific Computing at the University of Frankfurt/Main and the TKM computation cluster at the University of Karlsruhe.

Appendix A: Multi-Grid discretization

To employ the FFT algorithm an equidistant grid is required, which is not compatible with having a very high resolution at small values of ψ ($\sim 10^{-9}$) to capture the

behavior in the vicinity of the SF-insulator transition, as well as simultaneously correctly describing the distribution at large values ($\psi \sim 1$). To circumvent this problem, we use a superposition of equidistant grids, which enables us to use the FFT algorithm on each of these grids individually (see Fig. 15). This procedure relies on the fol-

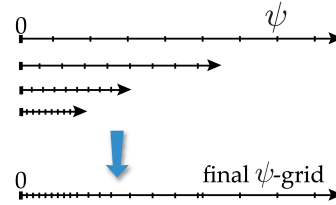


FIG. 15: Illustration of the multi-grid procedure.

lowing property of the convolution (4): the Z -fold convolution of the truncated function $P_t(\psi) = \Theta(a - \psi)P(\psi)$ with $P(\psi) = 0$ for $\psi < 0$ and $a < \psi_{\text{max}}/Z$ is identical to the Z -fold convolution of $P(\psi)$ up to an easily determinable normalization constant on the interval $[0, a]$. Here ψ_{max} is the largest value of the grid, if this is finite (as in the discretized numerical case). In our calculations the number of grids used (typically $\approx 1 \dots 6$) with $200 \dots 1000$ points per grid is adjusted dynamically within the iteration procedure, depending on the position of the most likely value of $P(\psi)$ and the convergence properties.

Appendix B: Numerical calculation of the CDF $F(\psi|\eta)$ for box disorder

We found the numerically most efficient method for calculating and tabulating the two-dimensional CDF $F(\psi|\eta)$ to be the following:

For every fixed value of η , consider the function (7) $g(\mu', \eta)$ on the interval $\mu' = (\mu - \epsilon) \in [\mu - \Delta/2, \mu + \Delta/2]$. We define the local minima and maxima of this function (including the end points) in increasing order as $\{\mu_1^{\text{min}}, \mu_2^{\text{min}}, \dots\}$ and $\{\mu_1^{\text{max}}, \mu_2^{\text{max}}, \dots\}$. Furthermore the n -th monotonically increasing and decreasing function on the restricted interval, provided that this interval exists, is denoted by

$$g^{(\text{inc}, n)}(\mu', \eta) = g(\mu', \eta) \quad \text{for } \mu' \in (\mu_n^{\text{min}}, \tilde{\mu}_n^{\text{max}}) \quad (\text{B1})$$

$$g^{(\text{dec}, n)}(\mu', \eta) = g(\mu', \eta) \quad \text{for } \mu' \in (\mu_n^{\text{max}}, \tilde{\mu}_n^{\text{min}}) \quad (\text{B2})$$

where

$$\tilde{\mu}_n^{\text{max}} = \min_m \{\mu_m^{\text{max}} | \mu_m^{\text{max}} > \mu_n^{\text{min}}\} \quad (\text{B3})$$

$$\tilde{\mu}_n^{\text{min}} = \min_m \{\mu_m^{\text{min}} | \mu_m^{\text{min}} > \mu_n^{\text{max}}\} \quad (\text{B4})$$

By construction, these functions are invertible in μ' within the defined range, allowing us to introduce the functions

$$h^{(\text{inc},n)}(\psi, \eta) = \begin{cases} 0 & \text{if } \psi \leq g(\mu_n^{\text{min}}, \eta) \\ (g^{(\text{inc},n)})^{-1}(\psi, \eta) - \mu_n^{\text{min}} & \text{if } \psi \in (g(\mu_n^{\text{min}}, \eta), g(\tilde{\mu}_n^{\text{max}}, \eta)) \\ 1 & \text{if } \psi \geq g(\tilde{\mu}_n^{\text{max}}, \eta) \end{cases} \quad (\text{B5})$$

$$h^{(\text{dec},n)}(\psi, \eta) = \begin{cases} 0 & \text{if } \psi \leq g(\tilde{\mu}_n^{\text{min}}, \eta) \\ \tilde{\mu}_n^{\text{min}} - (g^{(\text{dec},n)})^{-1}(\psi, \eta) & \text{if } \psi \in (g(\tilde{\mu}_n^{\text{min}}, \eta), g(\mu_n^{\text{max}}, \eta)) \\ 1 & \text{if } \psi \geq g(\mu_n^{\text{max}}, \eta) \end{cases} \quad (\text{B6})$$

in terms of which the CDF can be written as a superposition

$$F_\eta(\psi) = \frac{1}{\Delta} \sum_n \left(h^{(\text{dec},n)}(\psi, \eta) + h^{(\text{inc},n)}(\psi, \eta) \right) \quad (\text{B7})$$

Appendix C: PDF for a product of random variables

Including hopping disorder into the SMFT leads to the task of having to calculate the probability distribution for the newly defined random variable $\phi = J\psi$, if the PDFs for J and ψ are known functions $p_J(J)$ and $P(\psi)$. This can be done by taking the logarithm $s = \ln(\phi) = x + y$ and using the convolution theorem for the PDFs $P_x(x) = e^x P_J(e^x)$ (analogously for $P_y(y)$) of the random variables $x = \ln(J)$ and $y = \ln(\psi)$. The resulting distribution for ϕ can be denoted in compact form as

$$P_\phi(\phi) = \int dx P_J(e^x) P(\phi \cdot e^{-x}). \quad (\text{C1})$$

Using the FFT-algorithm for the numerical computation of this operation leads to a vast increase in performance, however it requires the functions $P_x(x)$ and $P_y(y)$ to be interpolated on an equidistant grid.

Appendix D: Compressibility in the insulating phases

In the special case with $P(\psi) = \delta(\psi)$, the disorder integration can be performed explicitly and expressions for the density and the compressibility can be found. Using partial integration and the property $\lim_{\epsilon \rightarrow \infty} p(\pm\epsilon) = 0$ for the on-site probability distribution, the disorder averaged density at finite temperature can be expressed as

$$\begin{aligned} \bar{n}(\beta, U, \mu, \Delta) &= \int d\epsilon p(\epsilon) \frac{\sum_{m=0}^{\infty} m e^{-\beta E_m(U, \mu - \epsilon)}}{\sum_{m=0}^{\infty} e^{-\beta E_m(U, \mu - \epsilon)}} \\ &= -\frac{1}{\beta} \int d\epsilon p(\epsilon) \frac{\partial}{\partial \epsilon} \left(\ln \sum_m e^{-\beta E_m(\mu - \epsilon)} \right) \\ &= \frac{1}{\beta} \int d\epsilon \frac{\partial p(\epsilon)}{\partial \epsilon} \left(\ln \sum_m e^{-\beta E_m(\mu - \epsilon)} \right) \end{aligned} \quad (\text{D1})$$

with $E_m(U, \mu') = Um(m-1)/2 - \mu'm$.

In the specific case of box disorder with

$$\frac{\partial p(\epsilon)}{\partial \epsilon} = \frac{1}{\Delta} [\delta(\epsilon + \Delta/2) - \delta(\epsilon - \Delta/2)] \quad (\text{D2})$$

the disorder averaged density takes on the form

$$\bar{n}(\beta, U, \mu, \Delta) = \frac{1}{\Delta\beta} \ln \left[\frac{\sum_m e^{-\beta E_m(\mu + \Delta/2)}}{\sum_m e^{-\beta E_m(\mu - \Delta/2)}} \right] \quad (\text{D3})$$

and the compressibility $\kappa = \frac{\partial \bar{n}}{\partial \mu}$ can be directly evaluated

$$\kappa = \frac{1}{\beta} \left(\frac{\sum_m m e^{-\beta E_m(\mu + \Delta/2)}}{\sum_m e^{-\beta E_m(\mu + \Delta/2)}} - \frac{\sum_m m e^{-\beta E_m(\mu - \Delta/2)}}{\sum_m e^{-\beta E_m(\mu - \Delta/2)}} \right). \quad (\text{D4})$$

For speckle disorder, on the other hand, one has

$$\frac{\partial p(\epsilon)}{\partial \epsilon} = \frac{\delta(\epsilon)}{\Delta} - \frac{\Theta(\epsilon)}{\Delta^2} e^{-\epsilon/\Delta} \quad (\text{D5})$$

and the compressibility takes on the form

$$\begin{aligned} \kappa &= \frac{1}{\Delta} \left[\frac{\sum_m m e^{-\beta E_m(\mu)}}{\sum_m e^{-\beta E_m(\mu)}} \right. \\ &\quad \left. - \frac{1}{\Delta} \int_0^\infty d\epsilon e^{-\frac{\epsilon}{\Delta}} \frac{\sum_m m e^{-\beta E_m(\mu - \epsilon)}}{\sum_m e^{-\beta E_m(\mu - \epsilon)}} \right]. \end{aligned} \quad (\text{D6})$$

Appendix E: Local Green's functions and DOS

To obtain the local DOS in an insulating phase, we calculate the single particle Green's functions

$$\begin{aligned} G^>(t) &= \langle b(t) b^\dagger(0) \rangle \\ G^<(t) &= \langle b^\dagger(0) b(t) \rangle \\ G(t) &= -i[\Theta(t) G^>(t) + \Theta(-t) G^<(t)] \end{aligned} \quad (\text{E1})$$

for local Fock states at finite temperature, where $b(t)$ is the on-site particle annihilation operator in the Heisenberg representation. The Fourier transformed Green's

function can be calculated and takes on the form

$$\begin{aligned}\tilde{G}(\omega) &= \int_{-\infty}^{\infty} dt e^{i\omega t} G(t) \\ &= \lim_{\gamma \searrow 0} \frac{1}{Z(\mu')} \sum_{m=0}^{\infty} e^{-\beta(\frac{U}{2}m(m-1) - \mu'm)} \\ &\quad \times \left[(m+1) \frac{\omega - Um + \mu' - i\gamma}{(\omega - Um + \mu')^2 + \gamma^2} \right. \\ &\quad \left. - m \frac{\omega - U(m-1) + \mu' - i\gamma}{(\omega - U(m-1) + \mu')^2 + \gamma^2} \right],\end{aligned}\quad (\text{E2})$$

where $Z(\mu) = \sum_{m=0}^{\infty} e^{-\beta(\frac{U}{2}m(m-1) - \mu m)}$ is the local partition function. This is related to the single particle DOS by

$$\begin{aligned}\rho(\omega, \mu') &= -\frac{1}{\pi} \text{Im}(\tilde{G}(\omega)) \\ &= \frac{1}{Z(\mu')} \sum_{m=0}^{\infty} e^{-\beta(\frac{U}{2}m(m-1) - \mu'm)} [(m+1) \\ &\quad \times \delta(\omega - Um + \mu') + m\delta(\omega - U(m-1) + \mu')].\end{aligned}\quad (\text{E3})$$

Averaging over the on-site energy distribution for speckle disorder leads to the final expression

$$\begin{aligned}\bar{\rho}(\omega, \mu, \Delta, \beta) &= \int d\epsilon p(\epsilon) \rho(\omega, \mu - \epsilon) \\ &= \frac{1}{\Delta} \sum_{m=0}^{\infty} \frac{(m+1) \Theta(\omega - Um + \mu)}{Z(Um - \omega)} \\ &\quad \times e^{-\frac{\omega - Um + \mu}{\Delta} - \beta(m\omega - \frac{U}{2}m(m+1))} [1 + e^{-\beta\omega}],\end{aligned}\quad (\text{E4})$$

whereas for a box disorder distribution one obtains³⁷

$$\begin{aligned}\bar{\rho}(\omega, \mu, \Delta, \beta) &= \frac{1}{\Delta} \sum_{m=0}^{\infty} (m+1) \frac{\Theta(\frac{\Delta}{2} - |\omega - Um + \mu|)}{Z(Um - \omega)} \\ &\quad \times \left[e^{-\beta E_m(Um - \omega)} + e^{-\beta E_{m+1}(Um - \omega)} \right].\end{aligned}\quad (\text{E5})$$

Appendix F: Method of incorporating thermal fluctuations explicitly into SMFT

Instead of performing the thermal average before constructing the conditional probability distribution for ψ , the SMFT furthermore also allows to explicitly facilitate the thermal fluctuations of ψ in the probability distribution. We have not yet performed the numerical calculation, but will outline the procedure.

$$P(\psi|\eta) = \frac{d}{d\psi} \int d\epsilon p(\epsilon) \Theta \left[\psi - \frac{\text{Tr}(b e^{-\beta H(\eta, \epsilon)})}{\text{Tr}(e^{-\beta H(\eta, \epsilon)})} \right], \quad (\text{F1})$$

where $\Theta(x)$ is the Heaviside step function.

This can be formulated in the following way: for fixed external parameter η (hence *conditional* probability distribution) the on-site energy is randomly drawn from $p(\epsilon)$ and the resulting single site Hamiltonian is diagonalized. For the different eigenstates $|i(\epsilon, \eta)\rangle$ with eigenenergies E_i the respective expectation value $\langle i(\epsilon, \eta) | b | i(\epsilon, \eta) \rangle$ is calculated. Within the grand canonical ensemble, this expectation value has the probability $[\text{Tr}(e^{-\beta H(\eta, \epsilon)})]^{-1} e^{-\beta E_i}$ of occurring. This probability is uncorrelated to the probability of a certain on-site energy ϵ occurring. Expressing this mathematically, we obtain the explicit formula for the conditional probability distribution

$$\begin{aligned}P(\psi|\eta) &= \frac{d}{d\psi} \int d\epsilon p(\epsilon) \left[\text{Tr}(e^{-\beta H(\eta, \epsilon)}) \right]^{-1} \\ &\quad \times \sum_{i=1}^{\infty} e^{-\beta E_i(\eta, \epsilon)} \Theta[\psi - \langle i(\epsilon, \eta) | b | i(\epsilon, \eta) \rangle]\end{aligned}\quad (\text{F2})$$

Equivalently on a formal level, one may work with the cumulative conditional probability function

$$\begin{aligned}F(\psi|\eta) &= \int d\epsilon p(\epsilon) \left[\text{Tr}(e^{-\beta H(\eta, \epsilon)}) \right]^{-1} \\ &\quad \times \sum_{i=1}^{\infty} e^{-\beta E_i(\eta, \epsilon)} \Theta[\psi - g_i(\mu - \epsilon, \eta)]\end{aligned}\quad (\text{F3})$$

with

$$g_i(\mu - \epsilon, \eta) = \langle i(\epsilon, \eta) | b | i(\epsilon, \eta) \rangle. \quad (\text{F4})$$

To evaluate the expression

$$q_i(\psi) = \int d\epsilon f_i(\epsilon) \Theta(\psi - g_i(\mu - \epsilon, \eta)) \quad (\text{F5})$$

we perform a variable substitution

$$\epsilon \mapsto x_i(\epsilon) \quad (\text{F6})$$

and subsequently

$$dx_i = \underbrace{\frac{dx_i(\epsilon)}{d\epsilon}}_{f_i(\epsilon)} d\epsilon. \quad (\text{F7})$$

Using the central theorem of calculus one can explicitly construct

$$x_i(\epsilon) = \int_{-\infty}^{\epsilon} d\epsilon' f_i(\epsilon'). \quad (\text{F8})$$

Since

$$f_i(\epsilon) = p(\epsilon) \frac{e^{-\beta E_i(\epsilon, \eta)}}{\text{Tr}(e^{-\beta H(\epsilon, \eta)})} \quad (\text{F9})$$

is a non-negative function the monotonously increasing function $x_i(\epsilon) \leftrightarrow \epsilon_i(x)$ is invertible in the relevant range. The conditional cumulative density function can then be explicitly calculated from

$$F(\psi|\eta) = \sum_{i=1}^{\infty} \int dx \Theta(\psi - g_i(\mu - \epsilon_i(x)), \eta) \quad (\text{F10})$$

As in the SMFT for $T = 0$, the self-consistency condition reads

$$P(\psi) = \frac{d}{d\psi} \int_0^{\infty} d\eta Q(\eta) F(\psi|\eta), \quad (\text{F11})$$

where $Q(\eta)$ is the Z -fold convolved and rescaled function of $P(\psi)$ with the random variable $\eta = J \sum_{i=1}^Z \psi_i$. The conditional cumulative density $F(\psi|\eta)$ now also contains the thermal fluctuations explicitly in the distribution (i.e. they are not averaged over within the self-consistency loop), so the subsequent determination of $P(\psi)$ is identical to the previous cases.

-
- ¹ M. P. A. Fisher, P. B. Weichman, G. Grinstein, and D. S. Fisher, Phys. Rev. B **40**, 546 (1989).
² M. H. W. Chan, K. I. Blum, S. Q. Murphy, G. K. S. Wong, and J. D. Reppy, Phys. Rev. Lett. **61**, 1950 (1988).
³ M. Greiner, O. Mandel, T. Esslinger, T. W. Hänsch, and I. Bloch, Nature **415**, 39 (2002).
⁴ M. Lewenstein *et al.*, Advances in Physics **56**, 243 (2007).
⁵ D. Jaksch, C. Bruder, J. I. Cirac, C. W. Gardiner, and P. Zoller, Phys. Rev. Lett. **81**, 3108 (1998).
⁶ W. Hofstetter, J.I. Cirac, P. Zoller, E. Demler, and M.D. Lukin Phys. Rev. Lett. **89**, 220407 (2002).
⁷ G. Roati *et al.*, Nature **453**, 895 (2008).
⁸ B. Deissler *et al.*, Nat. Phys. **6**, 354 (2010).
⁹ R. Roth and K. Burnett, Phys. Rev. A **68**, 023604 (2003);
¹⁰ L. Fallani, J. E. Lye, V. Guarrera, C. Fort, and M. Inguscio, Phys. Rev. Lett. **98**, 130404 (2007).
¹¹ U. Gavish and Y. Castin, Phys. Rev. Lett. **95**, 020401 (2005).
¹² S. Ospelkaus, C. Ospelkaus, O. Wille, M. Succo, P. Ernst, K. Sengstock, and K. Bongs, Phys. Rev. Lett. **96**, 180403 (2006).
¹³ J. E. Lye, L. Fallani, M. Modugno, D. S. Wiersma, C. Fort, and M. Inguscio, Phys. Rev. Lett. **95**, 070401 (2005).
¹⁴ J. Billy *et al.*, Nature **453**, 891 (2008).
¹⁵ D. Clément, P. Bouyer, A. Aspect, and L. Sanchez-Palencia, Phys. Rev. A **77** 033631 (2008).
¹⁶ M. White *et al.*, Phys. Rev. Lett., **102** 055301 (2009).
¹⁷ M. Pasienski, D. McKay, M. White, B. DeMarco, arXiv:0908.1182 (2009).
¹⁸ W. Krauth, N. Trivedi, and D. Ceperley, Phys. Rev. Lett. **67**, 2307 (1991).
¹⁹ J. Kisker and H. Rieger, Phys. Rev. B **55**, R11981 (1997).
²⁰ K. Sengupta *et al.*, New Journal of Physics **9**, 103 (2007).
²¹ R.T. Scalettar, G.G. Batrouni, and G.T. Zimanyi, Phys. Rev. Lett. **66**, 3144 (1991).
²² N. Prokof'ev and B. Svistunov, Phys. Rev. Lett. **92**, 015703 (2004).
²³ L. Dang, M. Boninsegni, and L. Pollet, Phys. Rev. B **79**, 214529 (2009).
²⁴ L. Pollet, N.V. Prokof'ev, B. Svistunov and M. Troyer, Phys. Rev. Lett., **103**, 140402 (2009).
²⁵ V. Gurarie, L. Pollet, N. V. Prokofev, B. V. Svistunov, and M. Troyer, Phys. Rev. B **80**, 214519 (2009).
²⁶ D.-S. Lühmann, K. Bongs, K. Sengstock, and D. Pfannkuche, Phys. Rev. A **77**, 023620 (2008).
²⁷ S. Rapsch, U. Schollwöck, and W. Zwerger, Eur. Phys. Lett. **46**, 559 (1999).
²⁸ K. G. Singh and D. S. Rokhsar, Phys. Rev. B **46**, 3002 (1992).
²⁹ J. Wu and P. Phillips, Phys. Rev. B **78**, 014515 (2008).
³⁰ F. Kruger, J. Wu, and P. Phillips, Phys. Rev. B **80**, 094526 (2009).
³¹ D. B. M. Dickerscheid, D. van Oosten, P. J. H. Denteneer, and H. T. C. Stoof, Phys. Rev. A **68**, 043623 (2003).
³² J.K. Freericks and H. Monien, Phys. Rev. B **53**, 2691 (1996).
³³ D.S. Rokhsar and B.G. Kotliar, Phys. Rev. B **44**, 10328 (1991).
³⁴ W. Krauth, M. Caffarel, and J.-P. Bouchaud, Phys. Rev. B **45**, 3137 (1992).
³⁵ K. Sheshadri, H. R. Krishnamurthy, R. Pandit, and T. V. Ramakrishnan, Eur. Phys. Lett. **22**, 257 (1993).
³⁶ K. Sheshadri, H.R. Krishnamurthy, R. Pandit, T.V. Ramakrishnan Phys. Rev. Lett., **75** 4075 (1995).
³⁷ K. V. Krutitsky, A. Pelster, and R. Graham, New J. Phys. **8**, 187 (2006).
³⁸ U. Bissbort and W. Hofstetter, EPL **86**, 50007 (2009).
³⁹ B. DeMarco, C. Lannert, S. Vishveshwara, and T.-C. Wei, Phys. Rev. A **71**, 063601 (2005).
⁴⁰ G. Semerjian, M. Tarzia, and F. Zamponi, Phys. Rev. B **80**, 014524 (2009).
⁴¹ V. I. Yukalov and E. P. Yukalova, Phys. Part. Nucl. **31**, 561 (2000).
⁴² V. I. Yukalov, Phys. Rev. B **71**, 184432 (2005).
⁴³ V. I. Yukalov and R. Graham, Phys. Rev. A **75**, 023619 (2007).
⁴⁴ F. Gerbier, Phys. Rev. Lett., **99** 120405 (2007).
⁴⁵ B. Svistunov, Phys. Rev. B **54**, 16131 (1996).
⁴⁶ W. Press *et al.*, Numerical Recipes in C++: The Art of Scientific Computing. Cambridge University Press, second edition (2002).
⁴⁷ L. Dell'Anna, S. Fantoni, P. Sodano, A. Trombettoni, J. Stat. Mech. **11**, 11012 (2008).
⁴⁸ S.Q. Zhou and D.M. Ceperley, Phys. Rev. A **81**, 013402 (2010).
⁴⁹ A.M. Rey, G. Pupillo, and J.V. Porto, Phys. Rev. A **73**, 023608 (2006).
⁵⁰ D. McKay, M. White, M. Pasienski, B. DeMarco, Nature **453**, 76 (2008).
⁵¹ M. Greiner, PhD thesis, Ludwig-Maximilians-Universität München (2003).